Journal of Asian Earth Sciences 111 (2015) 138–160

Contents lists available at ScienceDirect

Journal of Asian Earth Sciences

journal homepage: www.elsevier.com/locate/jseaes

Neoproterozoic ophiolite and related high-grade rocks of the Baikal–Muya belt, Siberia: Geochronology and geodynamic implications

A. Kröner [a,b,*], A.A. Fedotova [c,d], E.V. Khain [c], A.A. Razumovskiy [c], A.V. Orlova [c,d], M.O. Anosova [d], V.I. Perelyaev [e], G.E. Nekrasov [c], D.Y. Liu [a,b]

[a] Beijing SHRIMP Centre, Institute of Geology, Chinese Academy of Geological Sciences, 26 Baiwanzhuang Road, 100037 Beijing, China
[b] Dept. of Geosciences, University of Mainz, 55099 Mainz, Germany
[c] Geological Institute, Russian Academy of Sciences, 7 Pyzhevsky per., 119017 Moscow, Russia
[d] Vernadsky Institute of Geochemistry and Analytical Chemistry, Russian Academy of Sciences, 19 Kosygin Street, 119991 Moscow, Russia
[e] Faculty of Geology, Irkutsk State University, 1 Karl Marx Street, 664003 Irkutsk, Russia

ARTICLE INFO

Article history:
Received 10 March 2015
Received in revised form 15 July 2015
Accepted 30 July 2015
Available online 7 August 2015

Keywords:
Baikal
Siberia
Zircon dating
Cathodoluminescence
Ophiolite
Granulite
Neoproterozoic

ABSTRACT

We report zircon for from ophiolitic and high-grade rocks of the Neoproterozoic Baikal–Muya belt of Siberia that occupies an arc-shaped area on the southeastern margin of the Siberian craton. It consists of arc-related plutonic, metavolcanic and metasedimentary rocks as well as fragmented ophiolites and high-grade metamorphic assemblages. Magmatic zircons from two plagiogranite dyke samples of the Mamakan ophiolite complex in the Sredne–Mamakan massif of the eastern Baikal–Muya belt yielded similar and concordant SHRIMP mean $^{206}Pb/^{238}U$ ages of 640.0 ± 4.1 and 650 ± 6 Ma, respectively, that reflect the time of dyke emplacement and from which we suggest an age of ca. 645 Ma as the most likely time of ophiolite formation.

Enderbitic gneisses of the North Baikal area, in the western part of the Baikal–Muya belt, contain complex zircon populations that reflect variable recrystallization, Pb-loss and metamorphic overgrowth during granulite-facies metamorphism. LA-ICP-MS dating of these zircons yielded inconclusive results that led us to undertake a detailed study of cathodoluminescence images combined with U–Pb SHRIMP dating. Well-preserved magmatic domains in zircons from enderbite sample 2821 yielded concordant results with a mean $^{206}Pb/^{238}U$ age of 640 ± 5 Ma, slightly higher but broadly comparable with the data obtained by LA-ICP-MS. The zircon populations of two more enderbitic gneiss samples are more complex, and their LA-ICP-MS data constitute broad swaths along concordia between ca. 840 and 600 Ma, reflecting two end-member isotopic components, namely an igneous crystallization event at ca. 800 Ma and a Pb-loss and recrystallization event at ca. 600 Ma. SHRIMP analyses of magmatic zircon domains of these samples yielded concordant data with identical mean $^{206}Pb/^{238}U$ ages of 826 ± 7.5 Ma and 826 ± 8 Ma, respectively, whereas low-U metamorphic rims crystallized at 640 ± 7 Ma. Newly crystallized ball-round metamorphic zircons in one sample produced a mean $^{206}Pb/^{238}U$ age of 640 ± 6 Ma. We suggest that the protoliths of the enderbitic gneisses crystallized at 826 ± 7.5 Ma and experienced granulite-metamorphism at 640 ± 6 Ma. The LA-ICP-MS analyses are fully compatible with this interpretation.

Our geochronological data and previously published ages for Neoproterozoic igneous rocks of the Baikal–Muya belt define two age groups at 830–780 and 650–640 Ma. We interpret that the older group reflects the evolution of a large arc system in the Baikal–Muya belt and the eastern Sayan–northwestern Mongolia region, whereas the younger group documents collision between the above arc system and the southern margin of the Siberian craton.

1. Introduction

The Central Asian Orogenic Belt (CAOB, Ural-Mongolian fold belt in earlier Russian publications) is located between the Precambrian cratons of Baltica, Siberia, Tarim and North China (Fig. 1). It consists of latest Mesoproterozoic to late Palaeozoic island arcs, ophiolites, ocean islands, accretionary complexes and

* Corresponding author at: Beijing SHRIMP Centre, Institute of Geology, Chinese Academy of Geological Sciences, 26 Baiwanzhuang Road, 100037 Beijing, China.
E-mail address: kroener@uni-mainz.de (A. Kröner).

http://dx.doi.org/10.1016/j.jseaes.2015.07.033
1367-9120/

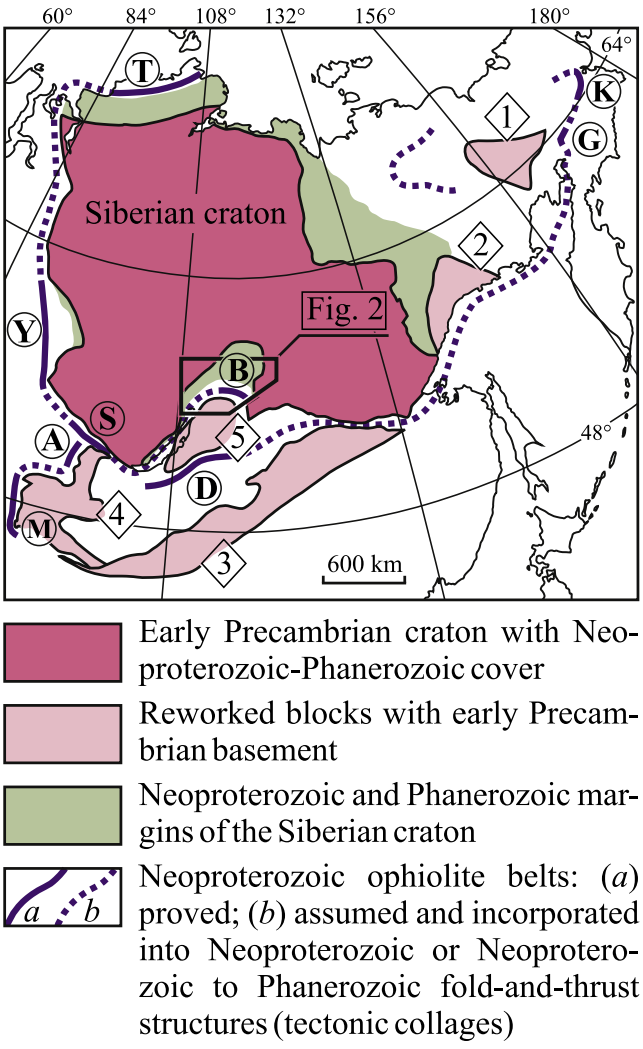

Fig. 1. Neoproterozoic (NP) ophiolite belts surrounding the Siberian craton (boundaries of the craton, continental blocks with early Precambrian basement and passive continental margins are mainly after Parfenov et al. (2010). Ophiolites incoporated within Neoproterozoic (NP) tectonic collages: T – Taimyr (Vernikovsky, 1996; Vernikovsky and Vernikovskaya, 2001), Y – Yenisey Range, Borisikha Massif (Kuzmichev et al., 2008); within NP-early Palaeozoic tectonic collages: S – Dariv-Shishkhid-Gargan zone in East Sayan Range: Dunzhugur Massif (Khain et al., 2002; Kuzmichev and Larionov, 2013), Shishkid Massif (Kuzmichev et al., 2005), M – the same zone in western Mongolia, Dariv and Khantaishir Massifs (Khain et al., 2003; Jian et al., 2014), A – Agardagh Tes-Chem ophiolite zone (Pfänder et al., 2002), B – Baikal–Muya zone (this paper); within Neoproterozoic-Palaeozoic structure: D – Dzhida (Gordienko et al., 2012) and Shaman complexes (Gordienko et al., 2009); within Mesozoic structures of the West-Koryak belt – K: Ust'-Bel'sky ophiolite complex (Tikhomirov, 2010) and related ultramafic rocks (Ledneva et al., 2012; Nekrasov and Bogomolov, 2015), and G – Ganychalan complex (Nekrasov and Makeev, 2003). Numbers in diamonds denote reworked blocks with early Precambrian basement: 1 – Omolon; 2 – Okhotsk; 3 – Argun; 4 – Central Mongolian; 5 – Barguzin.

more or less strongly reworked fragments of Archaean to Proterozoic continental massifs some of which preserve Neoproterozoic passive continental margin sequences. Many of these assemblages were tectonically dismembered during accretionary processes in the large archipelago-type Palaeo-Asian Ocean that ended in the late Palaeozoic when the numerous ocean bsins closed and collision occurred between the North China and Tarim cratons and the accreted terranes south of the Siberian craton (for reviews of the tectonic history see Wilhem et al., 2012; Kröner et al., 2014; Kröner, 2015).

The most ancient ophiolites and arc-related complexes of the CAOB surround the Siberian craton in the north (Taimyr Peninsula), southwest (Enisey Range), southwest (southern part of the East Sayan Range) and southeast (Baikalian mountain area) and constitute the Neoproterozoic Circum-Siberian Belt (Khain et al., 1997; Fig. 1). An eastern extension of this oceanic archipelago was discovered within the Cenozoic – Mesozoic domain of the northeastern margin of Asia, where remnants of Neoproterozoic ophiolites were identified (Khain et al., 1997). For example, the Ust'-Belaya ophiolite in the Koryak uplands (K in Fig. 1) contains tectonic blocks and sheets of different ages and origin. Plagiogranite from small veins in gabbro yielded a SHRIMP zircon age of 556 ± 17 (Tikhomirov, 2010), and amphibole gabbro from the same unit was dated at 799 ± 15 Ma (SHRIMP zircon age; Ledneva et al., 2012). Olivine pyroxenite from an adjacent thrust slice yielded a Sm–Nd mineral isochron age of 885 ± 83 Ma (Nekrasov and Bogomolov, 2015). The Ganychalan ophiolite complex is situated about 400 km to the southwest of the Ust'-Belaya terrane (G in Fig. 1) and contains amphibolites and gneisses from which zircons were dated at 532 ± 5 Ma (TIMS; Nekrasov and Makeev, 2003).

Neoproterozoic passive margin sequences are exposed along the present-day margins of the Siberian craton in the southwest (Enisey Range and the northern part of East Sayan Range, Sovetov et al., 2007; Sovetov, 2011), south and southeast (Baikalian mountain area, Patom uplands, Stanevich et al., 2007), and in the east (Yudoma-Maya area and Sette-Daban Range, Khudoley et al., 2001) (Fig. 1). These clastic-carbonate sequences unconformably overlie a Palaeoproterozoic metamorphic basement in the northern East Sayan Range (Sovetov, 2011) and in western Cisbaikalia (Gladkochub et al., 2013). They are mainly composed of clastic sedimentary rocks interlayered with carbonates and calcareous schists, mafic volcaniclastic rocks and glacial deposits. These successions reflect passive continental margin settings and tidal deposition on broad shelves recognized in detail on the southwestern margin of the Siberian craton between ca.750 and 540 Ma (Sovetov et al., 2007).

The Neoproterozoic history of the Circum-Siberian belt is recorded since about 1 Ga. A supra-subduction zone assemblage with an age of ca. 1020 Ma was revealed in the Dunzhungur ophiolite of East Sayan (Khain et al., 2002; Kuzmichev and Larionov, 2013), and by a 1017 ± 47 Ma subduction-related tonalite–trondhjemite suite identified in the Arzybey Complex in the northern part of East Sayan (Turkina et al., 2004). Metamorphosed N-MORB basalts (now amphibolites) were recognized in the roof zone of the Angaro-Vitim Batholith (Fig. 1) where an amphibolite was dated at 918 ± 15 Ma, a plagiogranite-gneiss associated with these amphibolites yielded an age of 972 ± 14 Ma (SHRIMP zircon studies, Nekrasov et al., 2007; Ruzhentsev et al., 2010), and a gabbro from this area yielded a SHRIMP zircon age of 939 ± 11 (Gordienko et al., 2009, 2010). Arc-related volcanic and ophiolitic sequences, formed at about 830–780 Ma ago, constitute an extensive belt in northern Mongolia and East Sayan (Kuzmichev et al., 2005; Kuzmichev and Larionov, 2011), and metavolcanic rocks, granites and gabbroic rocks with similar ages and with supra-subdution zone affinities occur in the Baikal–Muya belt (Izokh et al., 1998; Rytsk et al., 2001a,b) (Fig. 2). A Neoproterozoic active margin was also recognized in the Priolkhonie region (Fig. 1), based on zircon ages from a high-grade metamorphic complex (Gladkochub et al., 2010).

The Baikal–Muya belt consists of Neoproterozoic arc-related magmatic, metavolcanic and metasedimentary rocks, ophiolites and carbonates. It occupies an arc-shape area located between the margin of the Siberian craton (Baikal–Patom belt), and the Barguzin block (Fig. 2). It is situated in the northern part of the Baikal area and represents a Neoprotorozoic terrane that was slightly reworked during Palaeozoic magmatism. The geological events preserved in this belt provide data for the time interval

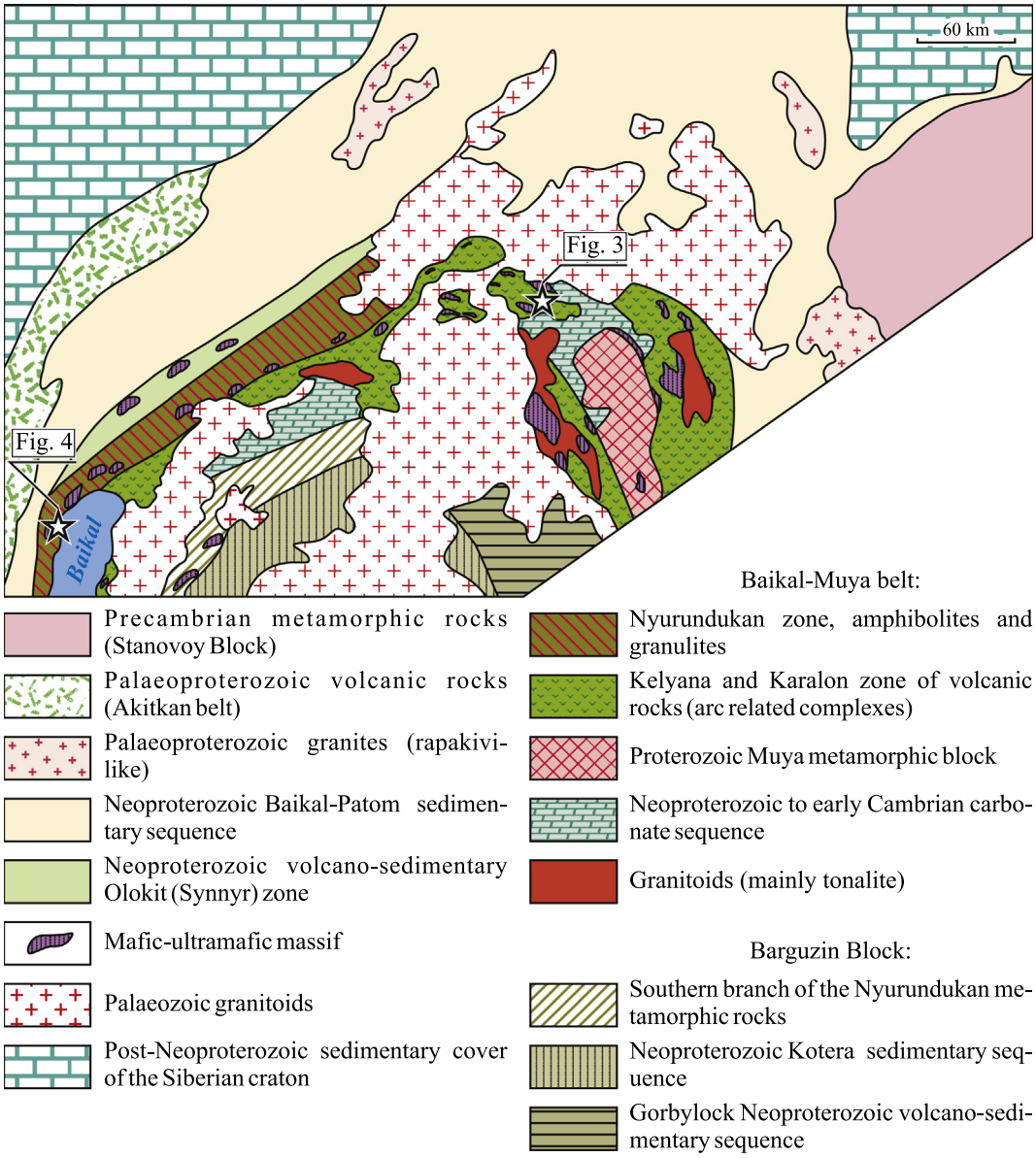

Fig. 2. Tectonic units of the Baikal mountain area, modified after Konnikov et al. (1999).

Table 1
Summary of sample localities, rock types, mineral compositions, and zircon ages for samples of this study (coordinates are in the WGS-84 system).

Sample	N. Latitude	E. Longitude	Locality and geological association	Rock type	Mineral composition	Age (Ma)
2768	56°57.20	114°26.77′	Unnamed right tributary of the Sredniy Mamakan River. Srednemamakan Massif (Fig. 3)	Plagiogranite	Plagioclase (partly replaced by sericite), quartz, amphibole	640.0 ± 4.1
2774	56°57.21′	114°26.77′	Unnamed right tributary of the Sredniy Mamakan River. Srednemamakan Massif (Fig. 3)	Plagiogranite	Plagioclase (partly replaced by sericite), quartz, amphibole	650 ± 6 850 ± 7
2821	55°24.90′	109°12.62′	Northern Cape Pisany Kamen. North Baikal high-grade complex (Fig. 4)	Enderbitic gneiss	Plagioclase, antiperthite, K-feldspar, cpx, opx (all partly altered)	640 ± 5
2914	55°22.96′	109°11.19′	Unnamed mountain 806 m, North Baikal high-grade complex (Fig. 4)	Opx-bearing gneiss	Orthopyroxene, plagioclase (partly replaced by saussurite)	826 ± 7.5 640 ± 7
AB2	55°22.84′	109°04.38′	Rel' River valley. North Baikal high-grade complex (Fig. 4)	Two-pyroxene gneiss	Orthopyroxene, clinopyroxene, plagioclase, quartz (<5%)	826 ± 8 640 ± 10

from 830 Ma to the late Neoproterozoic and are important to reconstruct the early history of the CAOB in southern Siberia.

The Baikal–Patom belt consists of a shallow-water shelf clastic-carbonate sequence including glacial deposits, interpreted as a Neoproterozoic passive margin sequence (Stanevich et al., 2007; Chumakov et al., 2007). In the inner part of the arc-shaped Baikal–Muya belt (Olokit and Bodaibo zones) a deep-water Neoproterozoic sedimentary sequence containing volcanoclastic

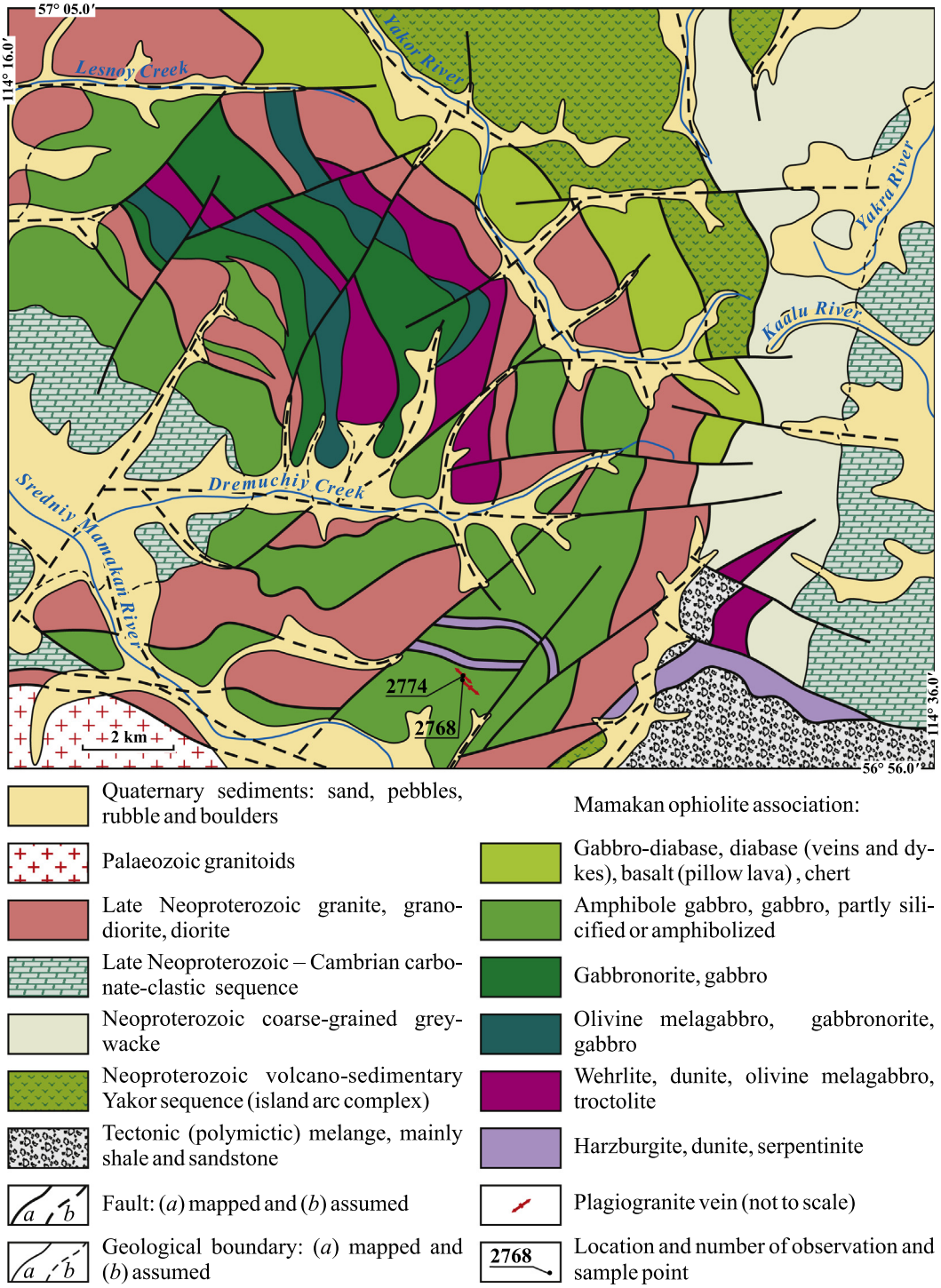

Fig. 3. Simplified geological map of the Mamakan ophiolite complex (after Perelyaev, 2003 and Stanevich and Perelyaev, 1997, for eastern part of area).

material and metavolcanic rocks is variably interpreted as a back-arc basin (Nemerov and Stanevich, 2001), a rift-related succession (Kuz'min et al., 2006) or an accretion prism (Zorin et al., 1995). In the Olokit zone (Fig. 2) these metasediments and metavolcanic rocks were intruded by the Dovyren gabbro massif dated at 707 ± 40 Ma (Sm–Nd mineral isochron) and at 730 ± 6 Ma (zircon, LA ICP-MS, Ariskin et al., 2013).

The Barguzin block is a strongly reworked heterogeneous terrane in the roof zone of the Angaro-Vitim Batholith and in adjacent areas including the Priolkhonie region. It contains a core of Archaen rocks (2670 ± 9.5 Ma), recognized in the eastern part of the block (Ruzhentsev et al., 2012), Mesoproterozic granites (Neymark et al., 1993), as well as Neoproterozoic ophiolites (Nekrasov et al., 2007; Gordienko et al., 2010) mentioned above, and Cambrian arc- related volcanic rocks (Ruzhentsev et al., 2010). Granulites occur in the Priolkhonie area and were dated at 498 ± 7 Ma (SHRIMP zircon age) and were interpreted to reflect collision of the Siberian craton with the Barguzin block (Gladkochub et al., 2008). The volcano-sedimentary sequence of the Katera zone (Fig. 2) and the Baikal metamophic belt (southern

Table 2
Major and trace element data for samples dated in this study and related rocks. Major elements in weight%, trace elements in ppm.

Object	Mamakan massif		North Baikal high grade complex					
Rock type	Ophiolitic plagiogranite		Pyroxene gneiss		Enderbitic gneiss		Metagabbro	Charnockitic gneiss
Sample #	**2768**	**2774**	**AB-2**	**2914**	**2821**	**2905-4**	**SB094B**	**2906**
SiO_2	73.99	72.57	54.31	63.83	57.17	57.66	47.55	75.57
TiO_2	0.16	0.21	0.93	0.78	1.29	1.23	2.07	0.29
Al_2O_3	14.83	14.92	18.98	15.61	18.17	18.55	15.34	11.90
Fe_2O_3	1.06	1.31	4.88	3.83	7.33	6.51	4.27	0.91
FeO			3.76	2.28			7.36	0.92
MnO	0.01	0.02	0.17	0.16	0.12	0.13	0.17	0.02
MgO	0.41	0.60	3.05	2.30	1.40	1.34	7.78	0.65
CaO	1.08	0.77	8.80	4.86	3.49	3.30	8.67	0.99
K_2O	1.03	0.78	0.80	1.11	4.41	4.75	1.96	5.47
Na_2O	6.29	7.39	3.56	4.08	4.83	4.92	2.95	2.82
P_2O_5	<0.03	0.04	0.34	0.25	0.31	0.35	0.38	0.04
LOI	0.96	0.79	0.00	0.68	1.11	0.62	0.70	0.30
Total	**99.81**	**99.40**	**99.58**	**99.75**	**99.63**	**99.36**	**99.19**	**99.89**
V	18.3	15.3	163.0	54.1	32.6	–	32.1	15.7
Cr	9.4	11.6	26.0	28.9	1.3	–	29.1	27.8
Mn	110	108	1147	1277	819	–	467	156
Co	2.2	2.1	24.6	8.95	11.1	–	6.10	2.29
Ga	19.9	20.3	20.6	18.1	22.9	22.4	25.8	14.8
Rb	35.80	21.00	3.11	11.5	26.40	28.63	5.35	92.7
Sr	214	180	610	331	467	600	724	87.5
Y	4.3	7.2	18.8	38.7	32.0	22.2	6.90	12.5
Zr	113	182	146	177	3068	300	335	134
Nb	6.65	11.60	3.18	5.41	20.7	17.9	2.31	3.52
Cs	1.54	0.41	0.08	0.08	0.15	0.25	0.44	0.38
Ba	548	368	414	515	3448	3636	520	266
La	16.8	28.9	15.9	21.7	34.6	27.0	20.5	47.6
Ce	29.7	57.4	33.8	48.9	71.3	52.7	32.9	93.3
Pr	2.64	5.09	4.40	6.39	9.00	6.94	3.42	9.52
Nd	8.4	15.8	18.9	27.4	37.8	27.9	12.1	31.5
Sm	1.02	2.44	4.09	6.27	7.68	5.75	1.97	5.04
Eu	0.29	0.39	1.38	1.76	5.93	6.61	2.60	0.553
Gd	0.92	1.56	3.87	6.44	7.08	5.79	1.59	3.87
Tb	0.117	0.216	0.603	1.06	1.07	1.094	0.223	0.551
Dy	0.70	1.25	3.69	6.82	6.12	4.45	1.28	2.87
Ho	0.130	0.244	0.772	1.51	1.33	0.916	0.276	0.535
Er	0.44	0.68	2.16	4.40	3.78	2.45	0.829	1.30
Tm	0.049	0.107	0.320	0.710	0.583	0.586	0.125	0.171
Yb	0.46	0.69	2.05	4.43	3.85	2.12	0.881	0.952
Lu	0.075	0.105	0.311	0.676	0.658	0.359	0.164	0.151
Hf	3.56	4.93	3.10	3.65	38.60	6.28	6.06	3.47
Ta	0.59	0.85	0.20	0.43	0.92	0.00	0.20	0.47
Th	13.2	10.9	0.30	0.44	0.28	0.27	0.36	15.3
U	2.82	1.75	0.06	0.09	0.40	0.17	0.25	0.88
La_n/Yb_n	26	29	5	3	6	9	16	35
Sr/Y	50	25	32	9	15	27	105	7
Eu/Eu*	0.9	0.6	1.1	0.8	2.4	3.5	4.5	0.4

branch of the Nurundukan metamorphic rocks in Fig. 2) mark the boundary between the Barguzin block and the Baikal–Muya belt (Rytsk et al., 2009). Late Palaeozoic granites of the Angaro-Vitim batholith (Yarmolyuk et al., 1997; Kovach et al., 2012) are widely distributed and obliterate many relationships between geological units of the Barguzin block.

The Baikal–Muya arc-shape belt is divided into western and eastern segments. The northwestern, outer part of the first segment is mainly composed of amphibolites, rare granulites and gabbros (Makrygina et al., 1989, 1993; Konnikov et al., 1999; Amelin et al., 2000; Tsygankov, 2005). These rocks make up a heterogeneus structure intruded by granitoids with adakite affinities at 595 ± 5 Ma (LA ICP-MS zircon study, Fedotova et al., 2014). The southern (inner) part of the western segment consists of late Neoproterozoic volcanic rocks and carbonates (Rytsk et al., 2007).

The eastern segment of the Baikal–Muya belt includes the Muya metamorphic block and surrounding arc-related units, ophiolites (Konnikov et al., 1994; Izokh et al., 1998; Rytsk et al., 2001a,b) and rift-induced magmatic series related to a transtensional setting (Tsygankov, 2005; Rytsk et al., 2011). A Sm–Nd mineral isochron age and zircon ages of these complexes are in a range 830–660 Ma (Izokh et al., 1998; Rytsk et al., 2001a,b). The Muya block has a heterogeneous structure including paragneiss, garnet-pyroxene-plagioclase-quartz gneiss, garnet-clinopyroxene-plagioclase-carbonate rocks and amphibolite, intercalated with carbonate rocks (Salop, 1964). An eclogite-facies mineral paragenesis is preserved in metagabbro and mafic rocks forming a blocks within two-mica, biotite and garnet gneisses in the North Muya block (Shatskii et al., 1996; Shatsky et al., 2012). A Sm–Nd (clinopyroxene, garnet and whole-rock) isochron yielded an age of 631 ± 17 for an eclogite sample, and garnet, magnetite and whole-rock analyses define the Sm–Nd isochron corresponding to an age of 636 ± 9 Ma for the host garnet gneiss (Shatsky et al., 2012). Whole-rock depleted mantle Nd model ages for these eclogites and gneisses are 0.7 and 1.6 Ga respectively (Shatsky et al., 2012).

Neoproterozoic ophiolites covering a wide age range from 939 ± 11 Ma (Gordienko et al., 2010) to 704 ± 71 Ma (Rytsk et al., 2001a,b) are exposed in the Baikal mountain area (Barguzin block

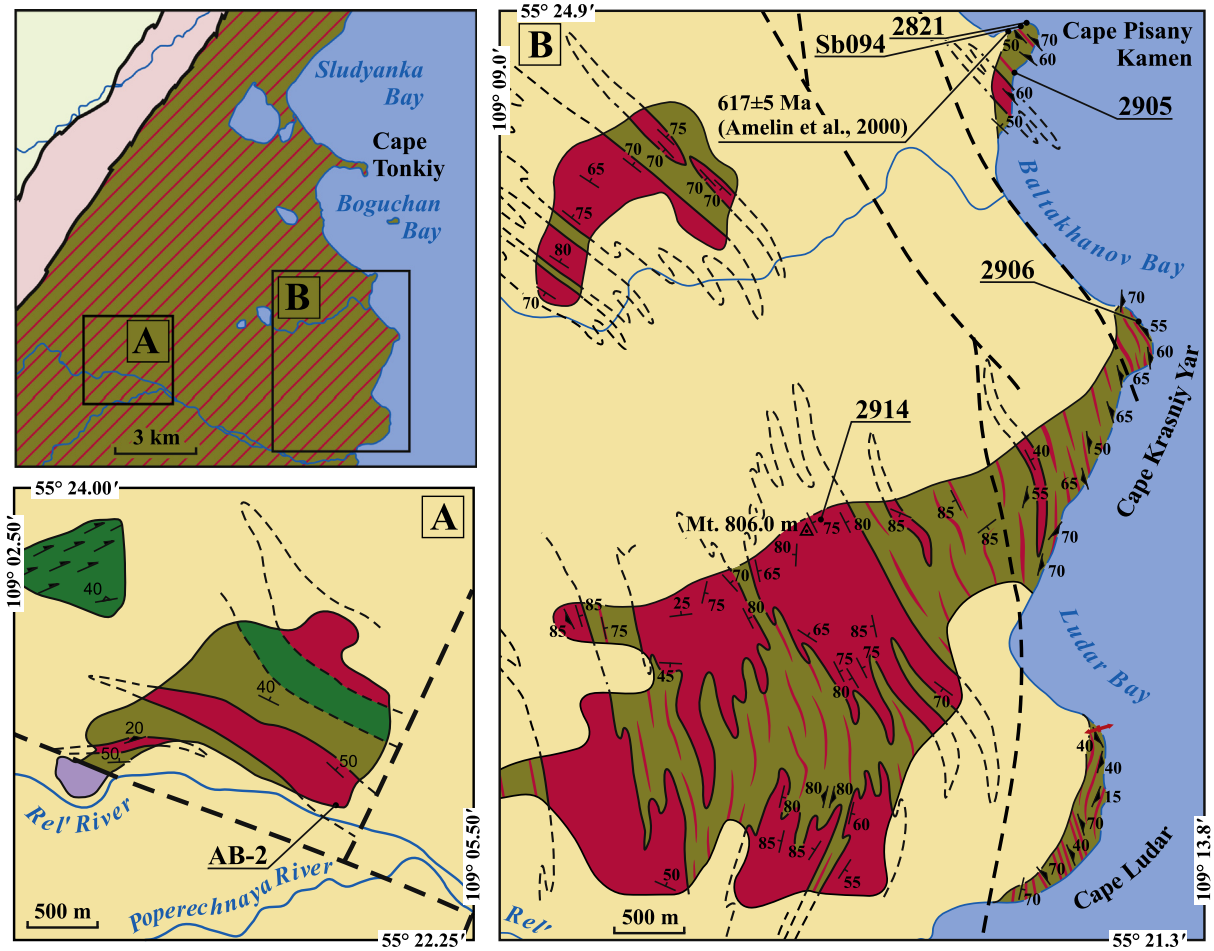

Quaternary sediments: clay, loam, sand, pebbles, rubble and boulders

Unspecified greenschist, amphibolite, limestone, gneiss of Olokit Zone

Tectonite, mylonite and blastomylonite

Fault: (*a*) mapped and (*b*) assumed

Geological boundary: (*a*) mapped and (*b*) assumed

Strike and dip: (*a*) primary (magmatic) compositional layering, (*b*) metamorphic banding and (*c*) contact of magmatic body and foliation

2821 Location and number of observation and sample point

Neoproterozoic rocks of the Baikal-Muya Belt:

Undifferentiated rocks

Two-pyroxene gneiss, amphibolite and amphibolitized gabbro

Leucocratic gneiss, enderbite and charnockite

Gabbro, amphibole gabbro, gabbronorite, olivine gabbro and troctolite

Peridotite with veins of gabbro

Amphibolitized gabbro

Granodiorite, leucogranite and sporadic garnet-bearing trondhjemite; not to scale

Fig. 4. Main tectonic units on the western shore of Lake Baikal and north of the Rel' River, and schematic geological maps of the Poperechnaya–Rel' junction area (A) and Baikal shore between Cape Pisany Kamen' and Cape Ludar (B), after Fedotova et al. (2014). (1) Quaternary sediments; (2) unspecified greenschist, amphibolite, limestone, gneiss of Olokit Zone; (3) tectonite, mylonite, and blastonylonite; (4–10) Neoproterozoic rocks of the Baikal–Muya belt: (4) unspecified, (5) two-pyroxene gneiss, amphibolite, and amphibolitized gabbro; (6) leucocratic gneiss, enderbite, and charnockite; (7) gabbro and amphibole gabbro, (8) gabbro, gabbronorite, olivine gabbro, and troctolite; (9) amphibolitized gabbro, (10) granodiorite, leucogranite, and sporadic garnetiferous tonalite bodies (a) at scale and (b) out of scale; (11) fault: (a) mapped; (b) inferred; (12) geological boundaries and structural trend lines: (a) mapped; (b) inferred; (13) strike and dip symbols: (a) primary (magmatic) mineral layering, (b) metamorphic banding, (c) contact of magmatic bodies, mineral foliation; (14) location and number of studied sample.

and Baikal–Muya belt), and these rocks are mainly metamorphosed and strongly dismembered. High-grade metamorphic rocks dated at about 490 Ma were described along the southern part of the Siberian craton from the Priolkhonie area (Gladkochub et al., 2008), and the question arises whether these rocks continue along the southeastern margin of the craton. A sample of enderbite was dated at 618 ± 5 Ma (TIMS analysis of 5 small zircon fractions), and the result was interpreted to date the beginning of retrogression after granulite-facies metamorphism (Amelin et al., 2000). The scale of distribution of high-grade rocks in the Baikal–Muya belt remains unknown. The location of our dated samples, their geological association, rocky type, mineral composition, and age are summarized in Table 1.

2. Geological relationships of the dated samples

2.1. Mamakan ophiolite complex

The Mamakan ophiolite complex (Stanevich and Perelyaev, 1997; Perelyaev, 2003) is located along the Yakor-Kaalu zone (Fig. 3) and is divided into the Kaalu ultramafic and Sredne–Mamakam ultramafic–mafic massifs. The Kaalu massif is composed of several tectonic blocks and lenses of serpentinized dunite and harzburgite enclosed in a polymict tectonic mélange, exposed on the watershed of the Kaalu and Sredniy Mamakan Rivers (Fig. 3). The ultramafic Kaalu massif is tectonically overlain in the southwest by a small tectonic lens composed of arc-related volcanic rocks of the Yakor unit (for details see Stanevich and Perelyaev, 1997).

Peridotite and layered gabbro of the Kaalu Massif are exposed in the Sredne–Mamakan block that covers an area of about 100 km^2 between the Sredniy (=middle) and Pravyi (=right) Mamakan Rivers (Fig. 3) and consists of a package of tectonic slices. In the south and southeast the Sredne–Mamakan Massif is unconformably overlain by a Vendian-Cambrian sedimentary sequence containing chromite-bearing sediments that were described as indicating erosion of ultramafic–mafic rocks (Perelyaev, 2003). The northwestern boundary of the peridotite-gabbroic block is a tectonic contact with basalt of the ophiolite association. The layered complex of the Sredne–Mamakan block includes veins and dykes of hornblende-pyroxene melagabbro, gabbro, microgabbro, and thin veins of websterite, plagiogranite and plagioclasite.

Light grey plagiogranite makes up rare veins in the layered gabbro and was sampled for age dating. Sample 2768 (Table 1, Fig. 3) was collected from a small vein (up to 40 cm wide) and sample 2774 represents another vein (up to 60 wide) from the same outcrop (Table 1, Fig. 3). The distance between the two veins is about 25 m. The chemical composition of these two samples is shown in Table 2. Thin and deformed diabase dykes intrude the layered gabbro in the studied outcrop, and locally gabbro veins also intrude the diabase, thus proving the same time of crystallization for dykes and gabbro. We therefore interpret the sample location as the root zone of a sheeted dyke complex.

A diabase complex is exposed in the valley of the Yakor River and on the watershed of the Dremuchiy and Kaaly rivers. In the Dremuchiy River valley it occurs below a tectonic sheet of serpentinized ultramafic rocks. On the left side of the valley of the Bolshoy Yakor River the diabase complex shows similarities with parallel (sheeted) dykes. Pillow lavas with rare interlayers of volcaniclastic and sedimentary (jaspilite-type) rocks occur in the volcano-sedimentary part of the ophiolite association (Fig. 3). All subvolcanic and volcanic rocks are metamorphosed to

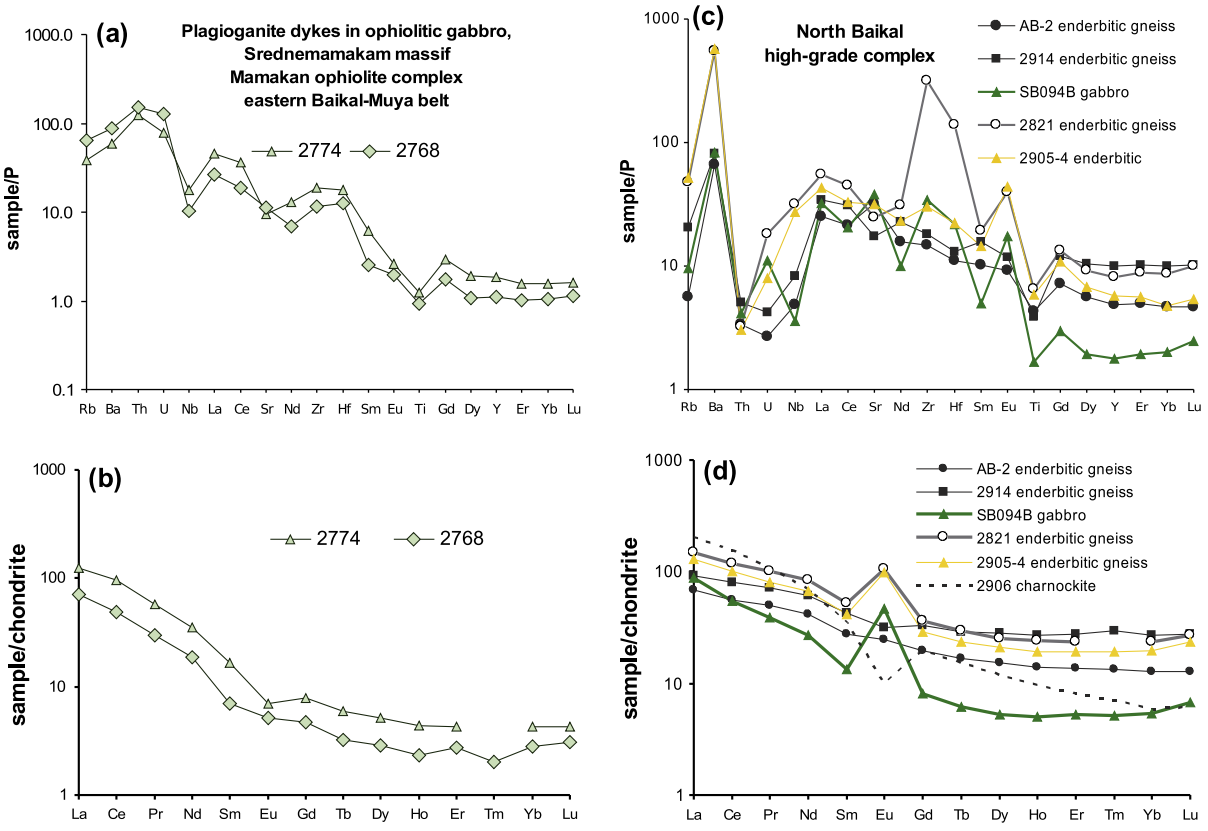

Fig. 5. Geochemical characteristics of rocks of this study and comparable samples. (A, C) are mantle-normalized trace element variation diagrams (normalizing values from Taylor and McLennan, 1985); (B, D) are chondrite-normalized rare earth variation diagrams (normalizing values from Anders and Grevesse, 1989). (A, B): Dated plagiogranite samples 2774 and 2768 compared with dyke samples 2793 and 2792 from adjacent areas and typical North Baikal tonalite sample SB072P17. (C, D): Dated enderbitic gneiss samples AB2 and 2914 compared with similar samples from adjacent areas (2905-4, SB094B) and K-rich granite sample 2906 from the North Baikal area.

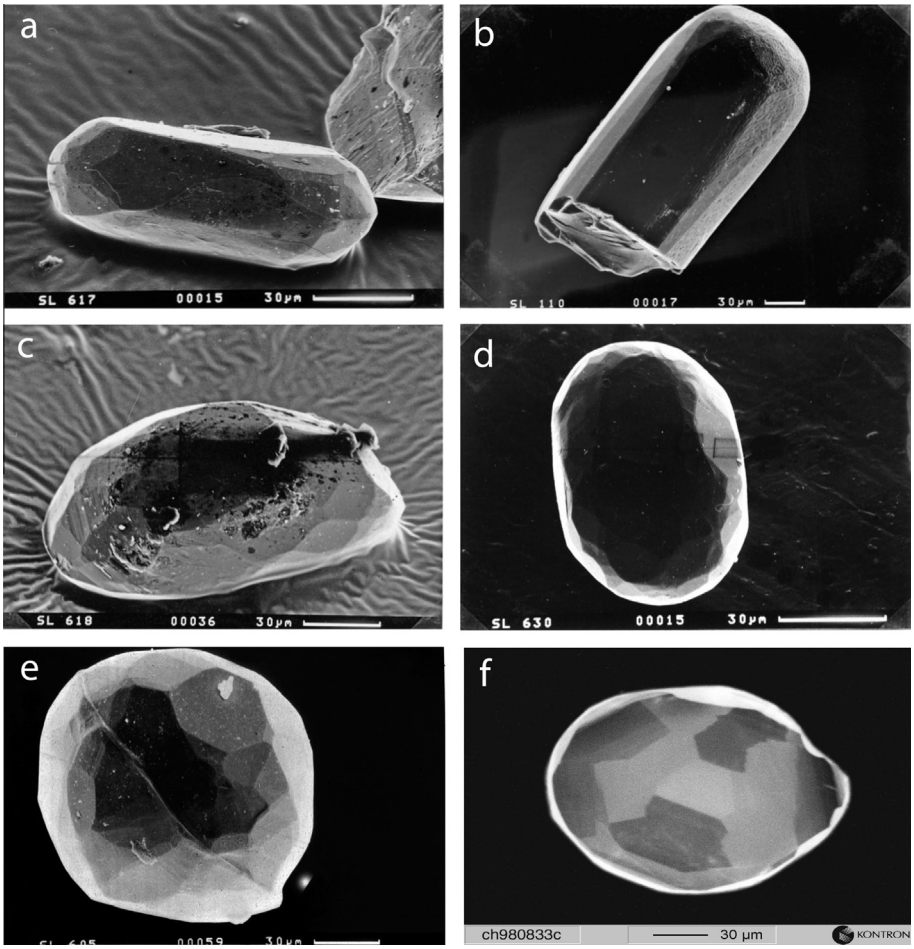

Fig. 6. Electron microscope photographs of zircon from medium- to high-grade metamorphic rocks of Sri Lanka and China. (a) Grain showing rounding at pyramidal terminations in amphibolite-facies granite-gneiss; (b) grain showing well-rounded and recrystallizerd termination with well-preserved small facets from granulite-facies granite-gneiss; (c) egg-shaped grain showing well rounded, recrystallized termination with many facets from granulite-facies granite-gneiss; (d) magmatic grain showing strong resorption and recrystallization with numerous facets in granulite-facies gneiss; (e) newly-formed metamorphic grain with large facets; (f) typical CL image of sectioned metamorphic grain from granulite in Hengshan Complex, China.

greenschist-facies or are completely altered and transformed to albite-chlorite-calcite mineral aggregates.

Our study area of the Sredne–Mamakan is mainly composed of high-Mg rocks with low or moderate Ti contents (Perelyaev, 2003). In the diagram CaO–MgO–Al_2O_3 the peridotite compositions plot along the line corresponding to fractionation of olivine – calcic plagioclase and orthopyroxene, whereas the data for the layered and upper gabbro plot along the line corresponding to the fractionation of clinopyroxene and plagioclase. The metabasalts can be subdivided into tholeiite containing MgO from 5.0 to 8.0 wt.% (average about 7.0 wt.%) and olivine basalt (MgO – 8–12 wt.% (average about 10 wt.%) and high-Mg basalt with more than 12.0 wt.% (for a range of 45–50 SiO_2 and FeO/MgO = 0.6–1.6). These rocks are interpreted to be back-arc basin basalts, and the Ti/1000 – V diagram (Shervais, 1983) shows that the basalts vary in composition from the N-type to E-type MORB. Ultramafic rocks and layered peridotite – gabbro units are enriched in Cr, Ni, and Co and show a positive correlation with MgO, due to fractionation of olivine and chromite. The ultramafic to mafic rocks are slightly enrichred in Rb, Ba, Cs, Th and La in relation to average N-MORB and show negative Nb and Zr anomalies. We consider that the origin of the Marmakan basalts is probably related to mixing of primary N-MORB-type magma with supra-subduction components. The distribution of REE in the igneous rocks confirms the above conclusion and suggests that they are formed from a slightly fractionated primary melt (La/Yb = 1.1–1.6; La/Sm = 0.8–1.1; Sm/Nd = 1.0).

The ophiolites are overlain by a Vendian (late Neoproterozoc) sequence of clastic sediments interpreted as molasse (Perelyaev, 2003). A Sm–Nd mineral isochron obtained for leuco-gabbro-norite from the gabbro-norite unit of the layered complex of the Sredne–Mamakan block yielded an imprecise age of 704 ± 71 Ma; whole-rock samples of clinopyroxenite and gabbro from layered anorthosite-gabbro unit define a Sm–Nd age of 774 ± 67 (Rytsk et al., 2001a,b).

Metavolcanic rocks of the easternmost segment (Tallai zone, Fig. 3) of the Baikal–Muya belt, located near the eastern side of the Muya metamorphic block, are correlated with volcanic rocks of the Sredne–Mamakan ophiolite complex or with the arc-related Yakor unit. In the Tallai River valley these rocks are seen to have been intruded by peridotite-pyroxenite-gabbro bodies, one of which, the Zaoblachnyi massif, yielded a Sm–Nd mineral isochron age of 612 ± 62 Ma (Izokh et al., 1998).

An eclogite of the North Muya metamorphic block provided a Sm–Nd isochron (garnet, clinopyroxene, whole-rock) age of 631 ± 17 Ma (Shatsky et al., 2012) that, within error, is identical to the above mineral isochron age obtained for the Sredne–Mamakam ophiolite complex (Rytsk et al., 2001a,b).

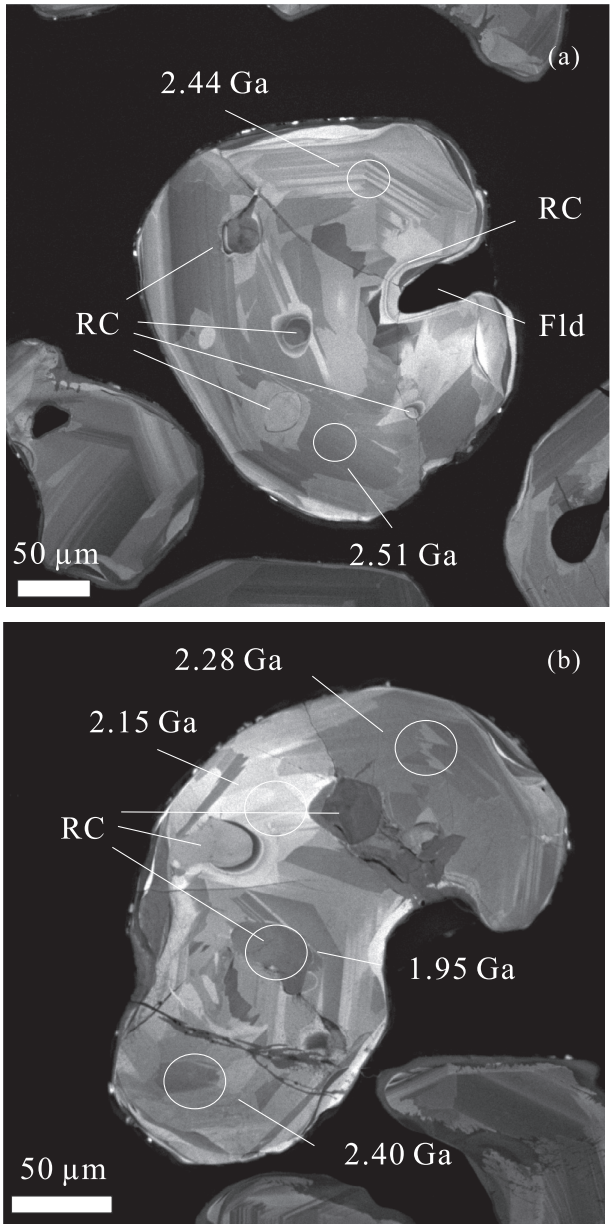

Fig. 7. Cathodoluminescence images for zircons from a cpx- and opx-bearing metadiorite gneiss of the high-grade late Archaean terrane in eastern Shandong, North China craton (Wan et al., 2011). These zircons show banded, fir-tree, sector- and/or oscillatory zoning. Positions of SHRIMP II analytical sites with ages (in Ga) are indicated. Note strong luminescence in small, local domains, probably due to recrystallization (RC). Palaeoproterozoic high-grade metamorphism at ca. 1.95 Ga (dark grey, recrystallized domains in a and b) has caused strong recrystallization of magmatic zircon (2.51 Ga, see b) and the formation of new metamorphic domains (b) Ages between 1.95 and 2.51 are due to mixing of igneous and metamorphic components.

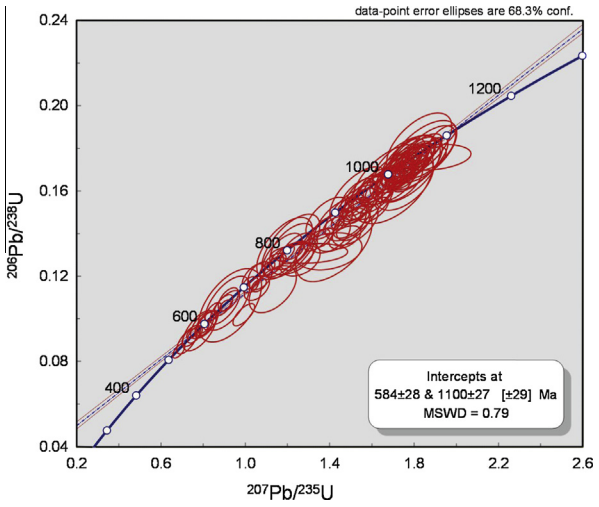

Fig. 8. Concordia diagram showing LA-ICP-MS analytical data for zircons from granulite-facies Vijayan Complex, southeastern Sri Lanka. Error ellipses are at 68.3% confidence. Note excellent linear distribution of isotopic ratios and two mean concordia intercept ages at 1100 ± 28 and 584 ± 28 Ma that define the maximim age of Vijayan magmatism and the peak of high-grade metamorphism as defined by both SHRIMP II and LA-ICP-MS dating (from Kröner et al., 2013).

2.2. High-grade gneiss terrane in the North Baikal region

Three complexes are represented in the study area of the North Baikal region (Fig. 4), namely (1) mafic granulites deformed together with two-pyroxene gneisses and gneisses of a magmatic enderbite-charnockite suite; (2) high-Ti gabbroic rocks (Slyudyanka massif) and low-Ti high-Al pyroxenite-troctolite-gabbro complex of the Tonkiy Mys massif; (3) a subvolcanic diorite-trondhjemite-granite complex intruding granulites and gabbroic rocks. The subvolcanic granitoids show adakite-like geochemical features (Fedotova et al., 2014), and high-Nb basalts were recently recognized in association with adakite-type granitoids (Khain et al., 2014).

Mafic granulites, two-pyroxene granulites, clinopyroxene gneisses as well as enderbitic and charnockitic gneisses are exposed in coastal cliffs and outcrops on the capes separating Boguchan, Baltakhanov, and Ludar Bays in the North Baikal area and are also exposed on the adjoining hills and in the Rel' River valley (Fig. 4). These high-grade rocks are deformed into tight folds with axes primarily trending in a northwestern and northern direction (Fig. 4A and B). The fold hinges are clearly seen in outcrops, in particular, in coastal cliffs and exposures at the eastern end of Boguchan Bay (Cape Pisany Kamen), in the northern part of Cape Ludar and on the upper part of the southeastern slope of the unnamed mountain with an 806 m mark (Fig. 4B). The valley of the Rel' River near the Poperechnaya River mouth is oriented along the fold axes (Fig. 4A).

Crystalline gneisses of the North Baikal area (two-pyroxene, clinopyroxene-, biotite–pyroxene or amphibole-pyroxene mafic rocks) were deformed together with enderbitic, charnockitic and two-pyroxene gneisses (Fig. 4). The products of retrograde metamorphism are biotite and amphibole–biotite schists and gneisses. Enderbites and two-pyroxene gneisses are similar looking, typically medium-grained rocks that are indistinguishable in the field. The temperature for granulite formation in the study area is 800–900 °C, and the pressure, according to the plagioclase-amphibole geobarometer, was 7.5–9 kbar (Tsygankov, 1996). A study of fluid inclusions in minerals of the charnoenderbite suite provided P–T estimates of 8–9 kbar and 800–900 °C.

The two-pyroxene and enderbitic gneisses, although difficult to distinguish in the field, show clear differences in their major and trace element geochemistry. The first are rocks with $Al_2O_3 > 15\%$, $TiO_2 < 0.9\%$ and relatively high levels of REE (Table 2) with slightly fractionationed patterns – $3 < La_N/Yb_N < 6$ and without clear Eu anomalies (Table 2, Fig. 5C and D). Negative Nb and Ti anomalies are shown in a multi-element variation diagram (Fig. 5C). The mafic granulites are characterized by similar REE patterns, but negative Nb anomalies are not prominent, and TiO_2 contents are high (1.8–4.0%). The two-pyroxene gneisses and mafic granulites both show low U and Th contents.

Enderbites are characterized by Al_2O_3 <15%, strong or moderately fractionated REE patterns ($8 < La_N/Yb_N < 33$) and a positive

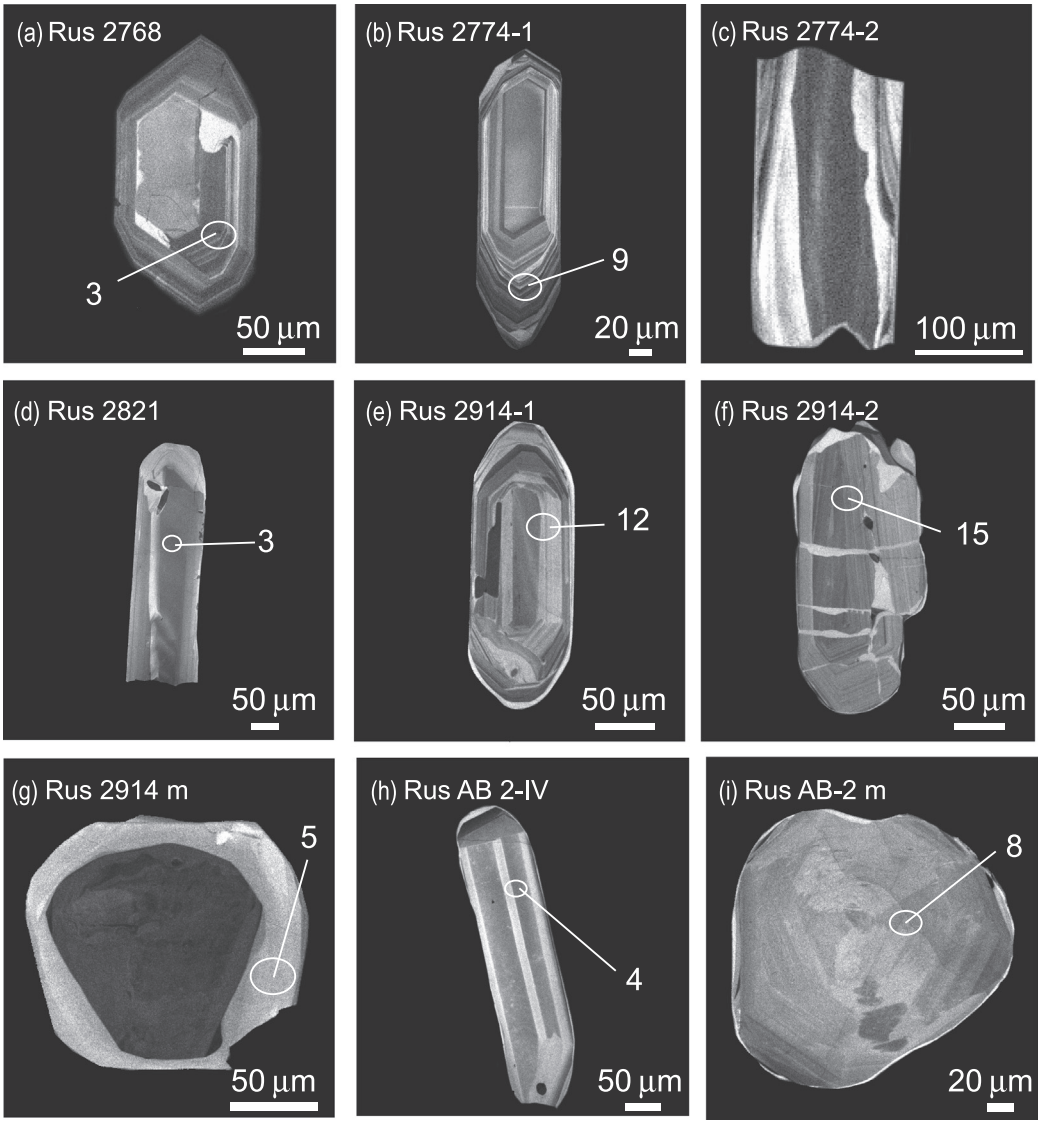

Fig. 9. Representative zircon CL images of zircon from dated samples of this study. (a) Idiomorphic magmatic grain from plagiogranite dyke sample 2768. (b) Concentric oscillatory-zones magmatic grain from plagiogranite sample 2774. (c) Striped zoning in magmatic grain from plagiogranite sample 2774. (d) Long-prismatic grain with rounded termination from enderbite sample 2821. (e) Magmatic grasin with both striped and oscillarory zoning and thin metamorphic overgrowth from enderbite sample 2914. (f) Magmatic grain with rounded termination and zircon-sealed fractures from enderbite sample 2914. (g) Igneous core with strong resorption surrounded by metamorphic rim from from enderbite sample 2914. (h) Long-prismatic grain with striped zoning from enderbite sample AB2. (i) Typical metamorphic grain with sector zoning from enderbite sample AB2.

Eu anomaly. Distinct negative anomalies of Eu, Nb, Ti are also present (Fig. 5C). The charnockites show similar geochemical characteristics (see sample 2906 in Table 2) except for the Eu anomaly – these rocks show Eu maximum at REE plots (Fig. 5C).

A mean $^{207}Pb/^{206}Pb$ age of 617 ± 5 Ma was obtained by conventional isotopic analysis of four air-abraided small zircon fractions from an enderbitic gneiss at Cape Pisany Kamen (Amelin et al., 2000, see Fig. 4). Zircons from samples 2914 and AB2 were dated by LA ICP-MS without the support of cathodoluminescence imagery, and the results show that zircons from these two samples contain inherited cores, and the rims probably crystallized at the same time as zircons from the surrounding granulites (Orlova et al., unpublished data). The analytical points plot in the interval 600–830 Ma, very close to Concordia, and probably define a discordia line, but the large errors prevent to calculate a concordia intercept age (Orlova et al., 2012). We shall present and discuss these data below together with our SHRIMP analyses.

Conventional U–Pb dating of magmatic zircons separated from a K-rich biotite granite-gneiss collected in the Rel' River valley (about 3 km from its mouth) provided three discordant analyses, and an age of 775 ± 15, obtained from a $^{207}Pb/^{206}Pb$ ratio, was interpreted to reflect the protolith age of the gneiss (Rytsk et al., 2013).

The aims of our geochronological study of enderbites from the North Baikal high-grade complex are to determine the upper age limit of the Nyurundukan suite, to understand the distribution of these high-grade rocks, and to define the time of high-grade metamorphism in the western part of the Baikal–Muya belt. Three samples were collected for zircon geochronology from different parts of study area (Fig. 4). Altered enderbitic gneiss sample 2821 (N 55°, 24.90′, E 109°, 12.62′) was collected from the coastal outcrop in the northern part of Cape Pisany Kamen from a sequence of interlayered enderbites and biotite-pyroxene or two-pyroxene mafic gneisses (Table 1, Fig. 4B). Partly altered orthopyroxene-bearing gneiss sample 2914 is from the upper part of the unnamed mountain peak 806.0 m; and unaltered two-pyroxene gneiss sample AB2 (N 55°, 22.84′, E 109°, 04.38′) was collected in the Rel' River valley (Table 1, Fig. 4A).

3. Morphological modification of zircon during prograde metamorphism and deformation

The zircon populations in the granulite-facies samples dated in this study show evidence of morphological modification and complex recrystallization during high-grade metamorphism. Kröner et al. (2014) documented the change in the morphology of magmatic zircon during progressive metamorphism in a series of high-magnification electron microscope photographs for grains from high-grade metamorphic rocks in Sri Lanka. In low-grade igneous rocks up to about middle amphibolite-facies the original eudral, prismatic shape of igneous zircon with its sharp pyramidal terminations is usually preserved, although rounding of these terminations may occur with increasing metamorphic grade (Fig. 6a) due to resorption by a zirconium-undersaturated intergranular fluid. Under high magnification the rounded terminations can be seen to be composed of numerous facets, showing the zircon to be recrystallized after resorption (Fig. 6b and c). This process of resorption may continue during amphibolite- to granulite-facies conditions so that the original pyramidal terminations become completely round and, if both ends of the zircon become rounded, the grain attains an oval shape (Fig. 11d). The process of resorption and recrystallization may continue to produce a variety of zircon morphologies, including egg-shaped grains that are particularly frequent in high-grade granitoid gneisses at the amphibolite- to granulite-facies transition. In extreme cases such grains may become ball-round and can then easily be mistaken for long-travelled detrital grains or metamorphic zircon.

Metamorphic zircon can usually be recognized under a binocular microscope, and distinguished from apatite, by its strong reflectivity, its "soccer-ball" shape (Vavra et al., 1996; Schaltegger et al., 1999; Kröner et al., 2000; Kröner, 2015), its multi-faceted surface (Fig. 6e), and its internal structure as revealed in CL images (Fig. 6f).

4. U–Pb isotopic data for zircons with complicated internal textures from high-grade rocks

Zircon populations from rocks with long and multiphase tectono-metamorphic histories generally do not consist of homogeneous crystals but may contain multiple components such as old cores, surrounded by magmatic overgrowth and further surrounded by metamorphic overgrowth. However, the robustness of zircon without radiation damage, even during ultra-high temperature metamorphism, and the insignificance of Pb-diffusion have been demonstrated in many studies, and careful CL- and trace element-assisted investigations make it possible to extract reliable age data from such grains (e.g., Möller et al., 2003; Kooijman et al., 2011). In contrast, fluid-induced alteration is common in zircon from high-grade metamorphic rocks (e.g., Geisler et al., 2007; Flowers et al., 2010; Wan et al., 2011; Dong et al., 2013; Ma et al., 2012; Kröner et al., 2015), and recrystallization, combined with Pb-loss, will produce variable discordance in a zircon population, particularly in granulite-facies assemblages (e.g., Corfu, 2013; Kröner et al., 2013; Kröner, 2015). Fig. 7 provides two examples of complex zircon showing evidence of recrystallization within small domains.

More severely discordant data are generally the result of either Pb-loss or mixing of two different zircon phases. Pb loss by recrystallization and/or redistribution, particularly under fluid conditions, often leads to partial or even complete isotopic resetting and no closed-system domains remain that can provide concordant ages. These cases are typical of high-grade metamorphic terranes where only discordant data can be extracted from many zircons (e.g., Corfu et al., 1994; Connelly, 2001; Moser et al., 2011). Such severe partial resetting by recrystallization and associated new growth results in linear arrays of data points in the concordia diagram between the time of crystallization and that of secondary reworking and/or local new growth (Moser et al., 2009; Kröner et al., 2013; Kröner, 2015; see Fig. 8).

A further problem related to zircon discordance concerns the interpretation of data that are nearly, but not fully, concordant. In many cases the slight discordance is due to ancient Pb loss, and the ages can then be extrapolated by projecting a line through the data from lower-intercept ages corresponding to the time of the supposed event (see Fig. 8). However, such events are often not evident from geological considerations, and such upper intercept extrapolations may thus be erroneous. In cases where the difference between the two concordia intercept ages is relatively small, the discordia line becomes subparallel to the concordia curve and, dependent on the magnitude of the uncertainty, indistinguishable from it (e.g., Corfu et al., 1994; Corfu, 2007; Kröner et al., 2013; see Fig. 8). Such cases are discussed below for zircons from Siberien enderbitic gneisses of this study.

An example is demonstrated in Fig. 8 where LA-ICP-MS data for zircons from granulite-facies gneisses in southeastern Sri Lanka plot between the igneous emplacement age at ca. 1100 Ma and a severe high-grade metamorphic event at 580 Ma (Kröner et al., 2013).

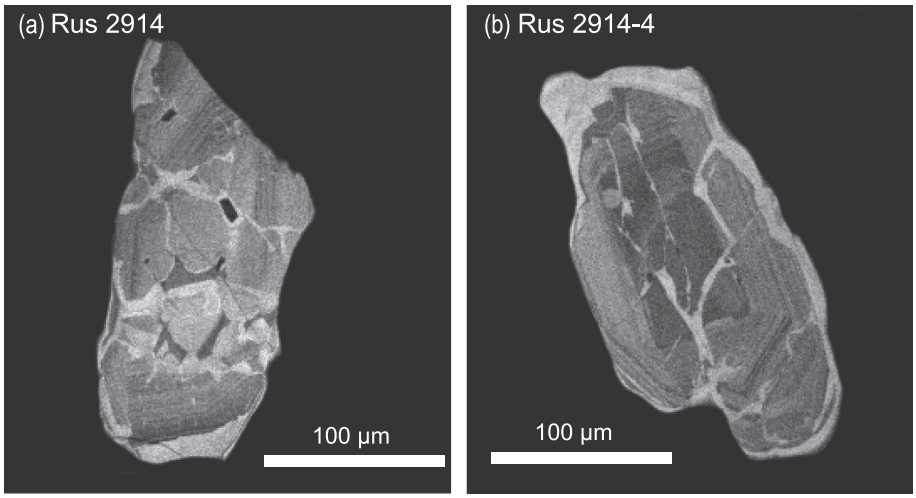

Fig. 10. CL images of fractured zircon grains from enderbite sample 2914. (a) Multiple fractures in magmatic zircon filled by highly luminescent (low-U) material. (b) Fractured grain showing fracture filling merging with metamorphic overgrowth rim.

Table 3
SHRIMP II analytical data for spot analyses of zircons from igneous rocks of the Baikal–Muya belt, Siberia.

Sample No.	U ppm	Th ppm	206Pb 204Pb	208Pb 206Pb	207Pb 206Pb	206Pb 238U	207Pb 235U	206/238 Age ± 1σ	207/235 Age ± 1σ	207/206 Age ± 1σ
2768-1	698	141	6526	0.0621 ± 23	0.0612 ± 10	0.1043 ± 13	0.880 ± 19	639 ± 7	641 ± 11	647 ± 37
2768-2	1418	590	27086	0.1240 ± 13	0.0607 ± 5	0.1043 ± 13	0.873 ± 14	640 ± 7	637 ± 7	629 ± 19
2768-3	848	319	15090	0.1129 ± 19	0.608 ± 8	0.1044 ± 13	0.876 ± 16	640 ± 7	639 ± 9	632 ± 27
2768-4	677	285	98912	0.1241 ± 10	0.0606 ± 4	0.1044 ± 13	0.872 ± 12	640 ± 7	636 ± 7	624 ± 14
2768-5	620	149	30012	0.0717 ± 13	0.0605 ± 6	0.1044 ± 13	0.870 ± 14	640 ± 7	636 ± 8	620 ± 21
2768-6	1206	536	35211	0.1311 ± 11	0.0607 ± 4	0.1043 ± 13	0.874 ± 13	640 ± 7	637 ± 7	629 ± 14
2768-7	1375	398	21997	0.0843 ± 9	0.0605 ± 4	0.1046 ± 13	0.872 ± 12	641 ± 7	636 ± 7	620 ± 13
2768-8	1066	185	29490	0.0531 ± 9	0.0607 ± 4	0.1044 ± 13	0.873 ± 13	640 ± 7	637 ± 7	628 ± 15
2774-1	468	427	12308	0.2723 ± 21	0.0671 ± 7	0.1409 ± 17	1.304 ± 22	850 ± 10	847 ± 10	842 ± 22
2774-2	340	55	8630	0.0495 ± 27	0.0610 ± 12	0.1057 ± 13	0.890 ± 21	648 ± 7	646 ± 11	641 ± 41
2774-3	978	331	19512	0.0996 ± 12	0.0608 ± 5	0.1065 ± 13	0.892 ± 14	652 ± 7	648 ± 7	631 ± 18
2774-4	310	159	9599	0.1512 ± 29	0.0674 ± 12	0.1411 ± 17	1.310 ± 30	851 ± 10	850 ± 13	849 ± 37
2774-5	385	514	3578	0.4979 ± 36	0.0612 ± 12	0.1062 ± 14	0.896 ± 23	651 ± 8	650 ± 12	647 ± 44
2774-6	373	81	10930	0.0614 ± 20	0.0614 ± 9	0.1061 ± 14	0.899 ± 18	650 ± 8	651 ± 10	654 ± 30
2774-7	182	117	4503	0.1872 ± 33	0.0670 ± 13	0.1407 ± 19	1.299 ± 32	849 ± 11	845 ± 14	837 ± 40
2774-8	169	113	6386	0.1900 ± 33	0.0665 ± 13	0.1411 ± 19	1.293 ± 32	851 ± 11	843 ± 14	821 ± 40
2774-9	253	185	1212	0.1905 ± 52	0.0666 ± 21	0.1410 ± 19	1.295 ± 46	850 ± 11	844 ± 21	825 ± 66
2774-10	460	158	31437	0.1028 ± 14	0.0612 ± 6	0.1060 ± 14	0.894 ± 15	649 ± 8	649 ± 8	646 ± 20
2774-11	218	41	89606	0.0596 ± 15	0.0616 ± 7	0.1061 ± 14	0.901 ± 17	650 ± 8	652 ± 9	661 ± 24
2774-12	142	50	1140	0.1254 ± 66	0.0686 ± 27	0.1411 ± 19	1.334 ± 58	851 ± 11	861 ± 25	886 ± 83
2774-13	173	122	2050	0.2209 ± 53	0.0677 ± 21	0.1410 ± 19	1.317 ± 47	850 ± 11	853 ± 20	860 ± 65
2821-1	63	44	7719	0.8667 ± 125	0.0607 ± 40	0.1045 ± 15	0.875 ± 61	641 ± 8	638 ± 33	628 ± 143
2821-2	74	53	3290	0.2298 ± 90	0.0642 ± 36	0.1049 ± 13	0.929 ± 55	643 ± 8	667 ± 29	749 ± 117
2821-3	125	88	1422	0.2202 ± 74	0.0638 ± 30	0.1046 ± 14	0.919 ± 46	641 ± 8	662 ± 24	734 ± 98
2821-4	65	46	4477	0.2116 ± 69	0.0637 ± 27	0.1042 ± 15	0.919 + 42	641 ± 8	662 ± 22	732 ± 89
2821-5	80	54	2772	0.2026 ± 96	0.0591 ± 39	0.1043 ± 14	0.850 ± 58	639 ± 8	625 ± 32	573 ± 142
2821-6	77	53	5843	0.2149 ± 72	0.0625 ± 28	0.1042 ± 15	0.899 ± 44	640 ± 8	651 ± 23	691 ± 96
2821-7	109	78	8394	0.2221 ± 107	0.0639 ± 43	0.1042 ± 14	0.918 ± 65	639 ± 9	661 ± 34	738 ± 144
2821-8	146	106	3640	0.2075 ± 47	0.0607 ± 18	0.1042 ± 14	0.873 ± 30	639 ± 8	637 ± 16	630 ± 65
2821-9	42	29	7452	0.1773 ± 210	0.0586 ± 86	0.1043 ± 14	0.843 ± 126	640 ± 10	621 ± 70	551 ± 325
2821-10	123	83	3037	0.2012 ± 59	0.0618 ± 23	0.1043 ± 14	0.889 ± 37	639 ± 8	646 ± 20	668 ± 81
2821-11	66	43	9027	0.1975 ± 116	0.0625 ± 47	0.1048 ± 15	0,903 ± 71	643 ± 9	653 ± 38	690 ± 161
2914-1	145	90	6135	0.1691 ± 38	0.0657 ± 16	0.1369 ± 18	1.240 ± 37	827 ± 10	819 ± 17	797 ± 52
2914-2	103	66	2753	0.1873 ± 63	0.0655 ± 27	0.1245 ± 17	1.124 ± 50	757 ± 10	765 ± 24	789 ± 85
2914-3	125	77	2792	0.1798 ± 51	0.0645 ± 22	0.1200 ± 16	1.068 ± 40	731 ± 9	738 ± 20	760 ± 71
2914-4	71	37	5234	0.1603 ± 107	0.0676 ± 45	0.1367 ± 20	1.275 ± 90	826 ± 11	834 ± 40	857 ± 139
2914-5	111	56	6509	0.1491 ± 39	0.0657 ± 17	0.1369 ± 19.	1.240 ± 38	827 ± 11	819 ± 17	795 ± 55
2914-6	183	111	81103	0.1843 ± 25	0.9644 ± 10	0.1201 ± 16	1.066 ± 24	731 ± 9	737 ± 12	754 ± 34
2914-7	97	42	16077	0.1334 ± 59	0.0662 ± 26	0.1238 ± 17	1.130 ± 48	752 ± 10	768 ± 23	814 ± 81
2914-8	113	61	5793	0.1599 ± 51	0.0659 ± 22	0.1368 ± 19	1.242 ± 46	827 ± 11	820 ± 21	802 ± 69
2914-9	20	8	7190	0.1183 ± 29	0.0652 ± 123	0.1045 ± 21	0.940 ± 181	641 ± 12	673 ± 95	781 ± 407
2914-10	27	53	109170	0.5783 ± 125	0.0617 ± 26	0.1044 ± 15	0.889 ± 42	640 ± 9	646 ± 22	665 ± 92
2914-11	15	32	3653	0.7346 ± 356	0.0679 ± 121	0.1045 ± 21	0.978 ± 178	640 ± 12	692 ± 91	865 ± 376
2914-12	161	97	5824	0.1715 ± 38	0.0687 ± 16	0.1367 ± 18	1.294 ± 37	826 ± 10	843 ± 17	889 ± 50
2914-13	39	91	6834	0.6857 ± 244	0.0594 ± 87	0.1045 ± 18	0.855 ± 128	641 ± 10	628 ± 70	581 ± 322
2914-14	184	120	12663	0.1942 ± 31	0.0669 ± 13	0.1367 ± 18	1.261 ± 31	826 ± 10	829 ± 13	835 ± 40
AB2ig-1	67	84	3390	0.3403 ± 98	0.0643 ± 37	0.1210 ± 17	1.072 ± 65	736 ± 10	740 ± 32	751 ± 122
AB2ig-2	77	102	3280	0.3907 ± 119	0.0604 ± 45	0.1044 ± 15	0.870 ± 67	640 ± 9	636 ± 36	620 ± 160
AB2ig-3	61	61	3685	0.3004 ± 74	0.0658 ± 27	0.1368 ± 19	1.242 ± 57	827 ± 11	820 ± 26	801 ± 87
AB2ig-4.1	233	246	6958	0.2998 ± 40	0.0655 ± 15	0.1365 ± 18	1.233 ± 34	825 ± 10	816 ± 15	790 ± 47
AB2ig-4.2	49	34	8556	0.1851 ± 178	0.0589 ± 74	0.1046 ± 17	0.849 ± 109	641 ± 10	624 ± 60	563 ± 275
AB2ig-5	24	37	1672	0.4003 ± 204	0.0653 ± 77	0.1171 ± 19	1.055 ± 128	714 ± 11	731 ± 63	784 ± 250
AB2ig-6	204	311	6104	0.4476 ± 44	0.0666 ± 14	0.1368 ± 18	1.256 ± 33	826 ± 10	826 ± 15	825 ± 44
AB2ig7.1	74	97	80645	0.3806 ± 55	0.0668 ± 15	0.1365 ± 19	1.256 ± 36	825 ± 11	826 ± 16	830 ± 48
AB2ig-7.2	44	53	1104	0.3405 ± 193	0.0635 ± 76	0.1042 ± 17	0.912 ± 112	639 ± 10	658 ± 60	726 ± 256
AB2ig-8	133	204	6456	0.4458 ± 66	0.0663 ± 23	0.1368 ± 19	1.252 ± 48	827 ± 11	824 ± 22	818 ± 71
AB2ig-9	51	55	22070	0.3057 ± 104	0.0643 ± 40	0.1163 ± 17	1.031 ± 67	709 ± 10	719 ± 34	751 ± 131
AB2m-1	23	23	8422	0.2891 ± 286	0.0650 ± 115	0.1049 ± 20	0.940 ± 170	643 ± 12	673 ± 89	773 ± 381
AB2m-2	39	65	1456	0.5017 ± 150	0.0579 ± 53	0.1043 ± 15	0.833 ± 79	639 ± 9	615 ± 44	527 ± 201
AB2m-3	24	51	7905	0.6473 ± 202	0.0667 ± 68	0.1042 ± 16	0.959 ± 101	639 ± 10	683 ± 52	829 ± 213
AB2m-4	65	73	1872	0.3142 ± 105	0.0611 ± 41	0.1048 ± 15	0.883 ± 61	643 ± 9	643 ± 33	642 ± 143
AB2m-5	24	19	1217	0.2328 ± 177	0.0633 ± 71	0.1044 ± 17	0.912 ± 105	640 ± 10	658 ± 56	719 ± 240
AB2m-6	42	54	3272	0.3953 ± 109	0.0632 ± 38	0.1041 ± 15	0.906 ± 57	638 ± 9	655 ± 31	713 ± 128
AB2m-7	23	51	4705	0.6559 ± 346	0.0588 ± 129	0.1042 ± 21	0.845 ± 188	639 ± 12	622 ± 104	561 ± 489

2768-1 is spot on grain 1, 2768-2 is spot on grain 2, etc.

If these two events were not known, the data could easily be interpreted as reflecting concordant ages implying multiple growth periods, and the possibility that individual sub-concordant data may be recording partial resetting or mixing is not always considered.

Data such as shown in Fig. 8 demonstrate Pb-loss or recrystallization, and since a precise correction for common Pb cannot be made for LA-ICP-MS data, it is often impossible to decide whether a particular analysis is concordant or slightly discordant. This is most relevant for Phanerozoic to Neoproterozoic zircons where it is customary to report $^{206}Pb/^{238}U$ ages. Such ages, if the data are discordant, are geologically questionable and almost always too low. This analytical problem can be overcome if different spots

Table 4
LA-ICP-MS data for zircons dated in this study.

No	Sample	Concentrations			Isotope ratios						Rho	Age (Ga)						Discord.
		Th (ppm)	U (ppm)	Th/U	$^{207}Pb/^{206}Pb$	Error 1σ	$^{207}Pb/^{235}U$	Error 1s	$^{206}Pb/^{238}U$	Error 1σ		$^{207}Pb/^{206}Pb$	Error 1s	$^{206}Pb/^{238}U$	Error 1σ	$^{207}Pb/^{235}U$	Error 1σ	
Panel a																		
1	2914-01	79	125	0.64	0.0660	0.0008	1.190	0.013	0.1308	0.0011	0.61	807	53	792	13	796	12	−0.5
2	2914-03	90	169	0.53	0.0634	0.0008	0.973	0.011	0.1114	0.0010	0.61	720	54	681	11	690	11	−1.3
3	2914-04	150	243	0.62	0.0666	0.0008	1.186	0.013	0.1293	0.0011	0.62	824	50	784	13	794	12	−1.3
4	2914-05	49	108	0.45	0.0657	0.0009	1.171	0.014	0.1294	0.0011	0.61	795	55	784	13	787	13	−0.4
5	2914-06	78	158	0.49	0.0657	0.0008	1.157	0.013	0.1278	0.0011	0.61	795	52	775	13	780	12	−0.7
6	2914-07	79	164	0.48	0.0664	0.0008	1.186	0.013	0.1296	0.0011	0.61	818	51	786	13	794	12	−1.1
7	2914-08	71	111	0.65	0.0656	0.0008	1.140	0.013	0.1260	0.0011	0.61	794	54	765	12	772	12	−1.0
8	2914-09	71	103	0.69	0.0659	0.0009	1.125	0.014	0.1238	0.0011	0.61	802	58	753	12	765	13	−1.7
9	2914-10	36	65	0.55	0.0640	0.0010	1.040	0.015	0.1179	0.0011	0.60	741	65	718	12	724	14	−0.8
10	2914-11	156	226	0.69	0.0653	0.0008	1.109	0.012	0.1232	0.0010	0.61	783	51	749	12	758	11	−1.1
11	2914-12	90	166	0.54	0.0648	0.0008	1.137	0.012	0.1273	0.0011	0.61	767	52	772	13	771	12	0.2
12	2914-13	119	195	0.61	0.0651	0.0008	1.114	0.012	0.1241	0.0011	0.61	777	51	754	12	760	11	−0.8
13	2914-14	89	164	0.54	0.0656	0.0008	1.152	0.012	0.1273	0.0011	0.61	794	51	773	12	778	12	−0.7
14	2914-15	61	127	0.48	0.0648	0.0008	1.043	0.012	0.1167	0.0010	0.61	768	54	711	12	725	12	−1.9
15	2914-18	32	75	0.44	0.0667	0.0008	1.219	0.015	0.1325	0.0014	0.64	829	53	802	15	809	14	−0.9
16	2914-19	77	151	0.51	0.0670	0.0008	1.244	0.014	0.1346	0.0013	0.65	839	47	814	15	821	12	−0.8
17	2914-20	76	134	0.56	0.0653	0.0007	1.162	0.013	0.1291	0.0013	0.65	784	47	783	14	783	12	−0.1
18	2914-21	94	146	0.65	0.0669	0.0007	1.244	0.013	0.1348	0.0013	0.65	835	46	815	15	821	12	−0.7
19	2914-22	98	182	0.54	0.0653	0.0007	1.158	0.013	0.1286	0.0013	0.65	785	48	780	15	781	12	−0.2
20	2914-24	33	49	0.68	0.0664	0.0009	1.186	0.015	0.1296	0.0013	0.63	817	55	786	15	794	14	−1.0
21	2914-27	63	130	0.49	0.0658	0.0007	1.175	0.013	0.1295	0.0012	0.64	801	47	785	14	789	12	−0.5
22	2914-28	63	103	0.62	0.0673	0.0008	1.217	0.014	0.1311	0.0013	0.64	847	51	794	15	808	13	−1.7
23	2914-30	215	355	0.61	0.0655	0.0007	1.189	0.013	0.1317	0.0013	0.65	790	46	798	15	796	12	0.2
24	2914-32	81	114	0.71	0.0656	0.0008	1.205	0.013	0.1333	0.0013	0.64	792	48	807	14	803	12	0.5
25	2914-33	73	142	0.51	0.0652	0.0008	1.110	0.013	0.1236	0.0012	0.64	779	49	751	14	758	12	−0.9
26	2914-34	81	133	0.61	0.0669	0.0008	1.203	0.014	0.1304	0.0013	0.64	835	49	790	14	802	12	−1.5
27	2914-35	100	194	0.52	0.0668	0.0008	1.200	0.013	0.1302	0.0012	0.64	833	47	789	14	801	12	−1.4
28	2914-36	93	145	0.64	0.0658	0.0008	1.150	0.012	0.1268	0.0012	0.64	800	48	770	14	777	12	−1.0
29	2914-37	120	170	0.71	0.0651	0.0007	1.140	0.014	0.1271	0.0015	0.69	777	45	771	17	773	13	−0.2
30	2914-38	53	111	0.48	0.0654	0.0007	1.218	0.015	0.1350	0.0016	0.69	789	45	817	18	809	14	0.9
31	2914-40	75	161	0.47	0.0669	0.0007	1.280	0.016	0.1388	0.0016	0.69	834	45	838	19	837	14	0.1
32	2914-41	104	163	0.64	0.0655	0.0007	1.179	0.014	0.1306	0.0015	0.69	790	45	792	17	791	13	0.1
33	2914-42	101	190	0.53	0.0663	0.0007	1.255	0.015	0.1374	0.0016	0.69	815	44	830	18	826	13	0.5
34	2914-43	108	156	0.69	0.0663	0.0007	1.241	0.015	0.1358	0.0015	0.69	816	45	821	18	820	13	0.1
35	2914-44	138	191	0.72	0.0643	0.0007	1.152	0.014	0.1300	0.0015	0.69	751	46	788	17	778	13	1.2
36	2914-46	107	189	0.56	0.0655	0.0007	1.166	0.014	0.1291	0.0015	0.68	790	45	783	17	785	13	−0.3
37	2914-47	109	187	0.58	0.0659	0.0007	1.224	0.015	0.1346	0.0015	0.68	805	46	814	17	811	13	0.3
38	2914-49	100	246	0.41	0.0655	0.0007	1.140	0.013	0.1263	0.0014	0.68	790	45	767	16	773	13	−0.8
39	2914-50	48	87	0.55	0.0673	0.0008	1.276	0.016	0.1375	0.0016	0.67	846	48	831	18	835	14	−0.5
40	2914-52	61	123	0.49	0.0643	0.0007	1.084	0.013	0.1224	0.0014	0.67	751	48	744	16	746	13	−0.2
41	2914-53	87	162	0.53	0.0656	0.0007	1.168	0.014	0.1292	0.0014	0.67	792	46	783	16	786	13	−0.3
42	2914-56	112	151	0.74	0.0658	0.0007	1.158	0.014	0.1276	0.0014	0.67	799	46	775	16	781	13	−0.8
Panel b																		
1	AB2u-1[a]	105	86	1.22	0.0629	0.0010	1.026	0.015	0.1182	0.0011	0.60	706	68	720	12	717	15	0.5
2	AB2u-2	133	125	1.06	0.0629	0.0010	0.926	0.013	0.1067	0.0010	0.60	706	66	654	11	666	14	−1.8
3	AB2u-3	41	45	0.91	0.0645	0.0014	1.122	0.023	0.1261	0.0012	0.58	759	89	766	13	764	21	0.2
4	AB2u-4	103	99	1.04	0.0643	0.0010	0.972	0.014	0.1097	0.0010	0.60	750	65	671	11	690	14	−2.7
5	AB2u-5	69	67	1.02	0.0649	0.0011	1.085	0.017	0.1212	0.0011	0.59	772	72	738	12	746	17	−1.1
6	AB2u-6	37	62	0.58	0.0662	0.0011	1.174	0.019	0.1285	0.0011	0.59	813	73	780	13	788	18	−1.1
7	AB2u-7	58	57	1.03	0.0633	0.0016	0.959	0.023	0.1098	0.0010	0.57	720	107	672	12	683	24	−1.6
8	AB2u-8	41	60	0.68	0.0644	0.0012	1.110	0.019	0.1250	0.0011	0.59	756	77	759	13	758	18	0.1
9	AB2u-9	58	82	0.72	0.0643	0.0011	1.000	0.016	0.1128	0.0010	0.59	751	71	689	11	704	16	−2.1

Table 4 (*continued*)

No	Sample	Concentrations			Isotope ratios						Rho	Age (Ga)						Discord.
		Th (ppm)	U (ppm)	Th/U	$^{207}Pb/^{206}Pb$	Error 1σ	$^{207}Pb/^{235}U$	Error 1s	$^{206}Pb/^{238}U$	Error 1σ		$^{207}Pb/^{206}Pb$	Error 1s	$^{206}Pb/^{238}U$	Error 1σ	$^{207}Pb/^{235}U$	Error 1σ	
10	AB2u-10	82	95	0.87	0.0648	0.0010	1.072	0.015	0.1200	0.0010	0.59	768	66	731	12	740	15	−1.2
11	AB2u-11	65	101	0.64	0.0662	0.0010	1.147	0.017	0.1256	0.0011	0.59	814	66	763	12	776	16	−1.7
12	AB2u-12	37	41	0.90	0.0663	0.0017	0.963	0.024	0.1054	0.0010	0.57	815	108	646	11	685	24	−5.7
13	AB2u-13	18	32	0.56	0.0659	0.0017	1.157	0.029	0.1274	0.0012	0.57	803	111	773	13	781	27	−1.0
14	AB2u-14	78	89	0.87	0.0646	0.0011	1.056	0.017	0.1185	0.0010	0.58	762	73	722	11	732	16	−1.3
15	AB2u-15	115	80	1.43	0.0618	0.0008	0.945	0.012	0.1109	0.0010	0.62	667	56	678	12	676	12	0.4
16	AB2u-16	107	88	1.21	0.0639	0.0008	1.008	0.012	0.1145	0.0011	0.62	737	54	699	12	708	12	−1.3
17	AB2u-17	77	77	1.00	0.0653	0.0008	1.147	0.014	0.1274	0.0012	0.62	783	54	773	13	776	13	−0.3
18	AB2u-18	63	57	1.10	0.0650	0.0009	1.009	0.014	0.1126	0.0010	0.61	774	60	688	12	708	14	−2.9
19	AB2u-19	84	75	1.12	0.0641	0.0008	1.121	0.014	0.1269	0.0012	0.62	745	55	770	13	764	13	0.8
20	AB2u-20	34	34	0.98	0.0639	0.0011	1.023	0.017	0.1162	0.0011	0.60	738	74	709	13	716	17	−1.0
21	AB2u-21	89	70	1.28	0.0619	0.0009	0.952	0.013	0.1115	0.0010	0.61	670	60	682	12	679	13	0.4
22	AB2u-22	38	47	0.82	0.0645	0.0011	1.037	0.016	0.1166	0.0011	0.61	757	70	711	13	722	16	−1.6
23	AB2u-23	98	93	1.06	0.0658	0.0009	1.082	0.014	0.1193	0.0011	0.62	799	58	727	13	745	14	−2.4
24	AB2u-24	33	38	0.87	0.0667	0.0011	1.123	0.018	0.1221	0.0011	0.60	829	69	743	13	764	17	−2.8
25	AB2u-25	25	34	0.73	0.0639	0.0011	1.079	0.018	0.1226	0.0012	0.60	737	75	746	13	743	18	0.3
26	AB2u-26	36	46	0.79	0.0656	0.0010	1.003	0.015	0.1109	0.0010	0.60	792	67	678	12	705	15	−3.8
27	AB2u-27	41	46	0.88	0.0642	0.0011	0.969	0.015	0.1094	0.0010	0.60	748	70	669	12	688	15	−2.7
28	AB2u-28	70	85	0.82	0.0620	0.0009	0.918	0.012	0.1074	0.0010	0.61	675	60	658	11	662	13	−0.6
29	AB2u-29	94	71	1.33	0.0608	0.0009	0.843	0.012	0.1005	0.0009	0.61	633	63	618	11	621	13	−0.5
30	AB2u-31	77	72	1.07	0.0656	0.0009	1.091	0.014	0.1207	0.0011	0.61	793	58	734	13	749	13	−2.0
31	AB2u-32	55	58	0.95	0.0672	0.0010	1.183	0.016	0.1277	0.0012	0.61	844	59	775	13	793	14	−2.3
32	AB2u-33	112	75	1.48	0.0599	0.0009	0.845	0.012	0.1023	0.0009	0.61	599	63	628	11	622	13	1.0
33	AB2u-35	155	116	1.33	0.0654	0.0008	1.071	0.013	0.1187	0.0011	0.62	788	54	723	12	739	12	−2.2
34	AB2u-36	37	42	0.89	0.0659	0.0011	1.176	0.018	0.1295	0.0012	0.60	802	67	785	14	790	16	−0.6
35	AB2u-37	38	75	0.51	0.0642	0.0009	1.043	0.013	0.1179	0.0011	0.61	747	59	718	12	725	13	−1.0
36	AB2u-38	50	49	1.03	0.0621	0.0011	0.894	0.014	0.1045	0.0010	0.60	677	72	641	11	649	15	−1.2
37	AB2u-40	141	114	1.23	0.0638	0.0008	1.112	0.013	0.1265	0.0011	0.62	734	54	768	13	759	12	1.1
38	AB2u-42	148	114	1.29	0.0650	0.0008	1.061	0.012	0.1183	0.0010	0.62	775	54	721	12	734	12	−1.8
39	AB2u-43	34	42	0.81	0.0657	0.0011	0.958	0.016	0.1057	0.0010	0.60	797	73	648	11	682	16	−5.0
40	AB2u-44	145	122	1.19	0.0664	0.0008	1.189	0.014	0.1299	0.0011	0.62	819	53	787	13	796	13	−1.0
41	AB2u-45	36	45	0.80	0.0636	0.0011	0.998	0.016	0.1139	0.0010	0.60	727	72	695	12	703	16	−1.1
42	AB2u-47	68	66	1.03	0.0620	0.0009	0.946	0.013	0.1107	0.0010	0.60	674	65	677	12	676	14	0.1
Panel c																		
43	AB2o-2[b]	111	131	0.85	0.0645	0.0007	1.079	0.014	0.1213	0.0015	0.70	759	47	738	17	743	14	−0.7
44	AB2o-3	72	73	0.98	0.0647	0.0008	1.033	0.014	0.1157	0.0014	0.69	766	50	706	16	720	14	−2.0
45	AB2o-4	6	64	0.09	0.0640	0.0008	1.062	0.015	0.1204	0.0015	0.68	741	51	733	17	735	14	−0.3
46	AB2o-5	69	88	0.79	0.0638	0.0008	1.052	0.015	0.1195	0.0015	0.69	736	50	728	17	730	14	−0.3
47	AB2o-6	33	45	0.73	0.0612	0.0008	0.910	0.014	0.1079	0.0013	0.67	645	58	661	15	657	14	0.5
48	AB2o-7	111	103	1.08	0.0642	0.0008	1.023	0.014	0.1156	0.0014	0.69	747	50	705	17	715	14	−1.4
49	AB2o-8	54	71	0.76	0.0650	0.0008	1.072	0.015	0.1195	0.0015	0.68	776	50	728	17	740	14	−1.6
50	AB2o-10	31	49	0.64	0.0656	0.0008	1.152	0.016	0.1274	0.0015	0.68	792	53	773	18	778	15	−0.6
51	AB2o-11	116	119	0.97	0.0649	0.0007	1.122	0.015	0.1253	0.0015	0.69	771	48	761	17	764	14	−0.3
52	AB2o-12	6	5	1.04	0.0621	0.0023	0.940	0.035	0.1098	0.0015	0.58	677	158	672	17	673	36	−0.2
53	AB2o-15	25	44	0.57	0.0648	0.0009	1.034	0.015	0.1157	0.0014	0.66	769	59	706	16	721	15	−2.1
54	AB2o-16	58	60	0.97	0.0641	0.0008	0.997	0.014	0.1129	0.0014	0.67	744	53	690	16	703	14	−1.8
55	AB2o-17	25	36	0.70	0.0655	0.0009	1.124	0.017	0.1245	0.0015	0.66	790	58	756	17	765	16	−1.1
56	AB2o-18	81	87	0.93	0.0653	0.0008	1.114	0.015	0.1237	0.0015	0.68	784	50	752	17	760	14	−1.1
57	AB2o-19	117	192	0.61	0.0654	0.0007	1.141	0.014	0.1264	0.0015	0.69	788	45	767	17	773	13	−0.7
58	AB2o-20	44	106	0.42	0.0657	0.0007	1.124	0.014	0.1240	0.0014	0.68	798	47	754	16	765	13	−1.5
59	AB2o-21	63	85	0.74	0.0632	0.0007	1.078	0.014	0.1237	0.0014	0.68	713	49	752	16	742	13	1.3
60	AB2o-22	112	95	1.18	0.0649	0.0007	1.117	0.014	0.1249	0.0015	0.68	771	49	759	17	762	14	−0.4
61	AB2o-23	130	193	0.67	0.0661	0.0007	1.153	0.014	0.1265	0.0014	0.68	810	45	768	16	779	13	−1.4
62	AB2o-24	61	63	0.97	0.0653	0.0008	1.070	0.014	0.1188	0.0014	0.67	785	51	724	16	739	14	−2.0

(*continued on next page*)

Table 4 (*continued*)

No	Sample	Concentrations			Isotope ratios						Rho	Age (Ga)						Discord.
		Th (ppm)	U (ppm)	Th/U	$^{207}Pb/^{206}Pb$	Error 1σ	$^{207}Pb/^{235}U$	Error 1 s	$^{206}Pb/^{238}U$	Error 1σ		$^{207}Pb/^{206}Pb$	Error 1 s	$^{206}Pb/^{238}U$	Error 1σ	$^{207}Pb/^{235}U$	Error 1σ	
63	AB2o-25	51	66	0.78	0.0644	0.0008	1.141	0.015	0.1286	0.0015	0.67	754	50	780	17	773	14	0.8
64	AB2o-27	79	71	1.10	0.0654	0.0008	1.137	0.014	0.1260	0.0014	0.67	789	50	765	16	771	14	−0.8
65	AB2o-29	42	52	0.80	0.0676	0.0009	1.119	0.015	0.1201	0.0013	0.66	856	53	731	15	763	14	−4.1
66	AB2o-30	81	81	1.00	0.0648	0.0008	1.068	0.013	0.1196	0.0013	0.67	767	50	728	15	738	13	−1.3
67	AB2o-31	33	33	1.00	0.0659	0.0009	1.066	0.015	0.1173	0.0013	0.65	803	58	715	15	737	15	−2.9
68	AB2o-32	27	39	0.70	0.0658	0.0009	1.163	0.016	0.1281	0.0014	0.66	801	55	777	16	783	15	−0.8
69	AB2o-33	43	56	0.76	0.0656	0.0008	1.126	0.015	0.1245	0.0014	0.66	794	53	757	16	766	14	−1.2
70	AB2-01	40	50	0.81	0.0610	0.0010	0.886	0.013	0.1054	0.0010	0.60	638	70	646	11	644	14	0.3
71	AB2-02	91	85	1.07	0.0634	0.0009	0.965	0.012	0.1104	0.0010	0.60	721	60	675	11	686	13	−1.6
72	AB2-03	81	67	1.20	0.0618	0.0009	0.894	0.012	0.1049	0.0009	0.60	668	64	643	11	649	13	−0.9
73	AB2-04	34	48	0.71	0.0630	0.0010	1.068	0.016	0.1229	0.0011	0.60	709	67	747	13	738	15	1.3
74	AB2-05	58	53	1.09	0.0643	0.0010	1.006	0.014	0.1135	0.0010	0.60	751	65	693	12	707	14	−2.0
75	AB2-06	42	37	1.13	0.0581	0.0011	0.781	0.014	0.0976	0.0009	0.59	533	82	600	11	586	16	2.4
76	AB2-07	54	43	1.24	0.0594	0.0010	0.820	0.013	0.1001	0.0009	0.59	582	76	615	11	608	15	1.2
77	AB2-09	56	49	1.15	0.0605	0.0010	0.814	0.012	0.0976	0.0009	0.60	622	71	600	10	605	14	−0.7
78	AB2-10	147	113	1.30	0.0651	0.0009	1.030	0.013	0.1147	0.0010	0.61	778	57	700	11	719	12	−2.6
79	AB2-11	31	44	0.71	0.0595	0.0010	0.828	0.013	0.1009	0.0009	0.59	585	73	620	11	612	14	1.2
80	AB2-12	52	26	2.03	0.0605	0.0012	0.829	0.016	0.0995	0.0009	0.58	620	88	611	11	613	18	−0.3
81	AB2-13	50	63	0.80	0.0618	0.0009	0.917	0.013	0.1077	0.0009	0.60	666	64	659	11	661	13	−0.2
82	AB2-14	47	60	0.79	0.0627	0.0009	0.985	0.013	0.1138	0.0010	0.60	699	63	695	12	696	13	−0.1
83	AB2-15	70	96	0.73	0.0630	0.0013	0.966	0.018	0.1112	0.0011	0.59	708	86	680	12	686	19	−1.0

[a] AB2u – elongated grains.
[b] AB2o – ball-shaped grains.

on a specific grain or several grains from the same sample are analyzed because it is unlikely that all grains or grain-domains contain the same amount of common Pb or experienced the same amount of Pb loss.

5. Zircon morphology and internal structure

5.1. Brief characterization of dated zircon populations based on CL images

We now briefly characterize the zircon populations dated in this paper in describing their CL images some of which are reproduced in Fig. 9. Plagiogranite sample 2768 contains a relatively simple igneous zircon population characterized by prismatic grains with perfectly preserved pyramidal terminations (Fig. 9a). Magmatic zoning varies from concentric, oscillatory to fairly broad as is typically seen in gabbroic rocks. Some grains have zoned interiors rimmed concordantly by very low luminescent (high-U) idiomorphic domains. A few grains show evidence of recrystallization, but this is overgrown by concentrically zoned domains (Fig. 9a), so this must have occurred during magmatic growth of the grains.

Plagiogranite sample 2774 also contains idiomorphic to slightly rounded magmatic zircon with well-preserved oscillatory (Fig. 9b) or striped zoning (Fig. 9c). Some grains show some recrystallization in their cores, overgrown by zoned domains, and a few grains have metamict patches in high-U domains. Although the CL-images are highly variable, the entire population looks magmatic in origin.

Enderbitic gneiss sample 2821 contains a uniform population of long-prismatic grains with well-rounded terminations and either broad, patchy or striped zonation (Fig. 9d), suggesting crystallization from a high-temperature and fairly homogeneous magma with respect to uranium and other trace elements. Recrystallization is evident in some grains containing low-luminescent patches or embayments cutting across the magmatic zonation. Clearly, this zircon population is of igneous origin.

The zircon population in the second enderbitic gneiss sample 2914 is very different in containing three different types of zircon. The most common type consists of well-preserved long-prismatic, oscillatory-zoned grains typical of granitic rocks with well-rounded terminations (Fig. 9e). Many grains have narrow, high-luminescent rims of likely metamorphic origin. Several grains of this population show evidence of fracturing with the cracks filled by the same zircon material as seen in the rims (Fig. 9f). This unusual feature in the second zircon type is further discussed below. The third type are oval to ball-round, often multifaceted grains. Most are oscillatory-zoned and most likely acquired their shapes during severe resorption. Thus they are of igneous origin but morphologically resemble metamorphic grains. Some of these have narrow to broad high-luminescent metamorphic rims (Fig. 9g).

The magmatic zircon population of enderbite sample AB2 is rather similar to that of 2821 in that most grains are long-prismatic with rounded terminations and striped zoning (Fig. 9h). There are also grains with rather homogeneous CL-patterns or irregular patches of various shades of light- to medium-grey. Rare grains have oscillatory zoning, and several have thin metamorphic rims. A few grains are well rounded due to severe resorption and have metamorphic rims. There are also numerous virtually ball-round, multifaceted grains with weak but typical sector-zoning or medium-grey, homogeneous CL patterns. These are undoubtedly grains that grew during high-grade metamorphism.

5.2. Fractured zircon

Unique to many grains from enderbite sample 2914 are narrow (up to 5–10 μm wide) zones of CL-bright zircon, which cross-cut

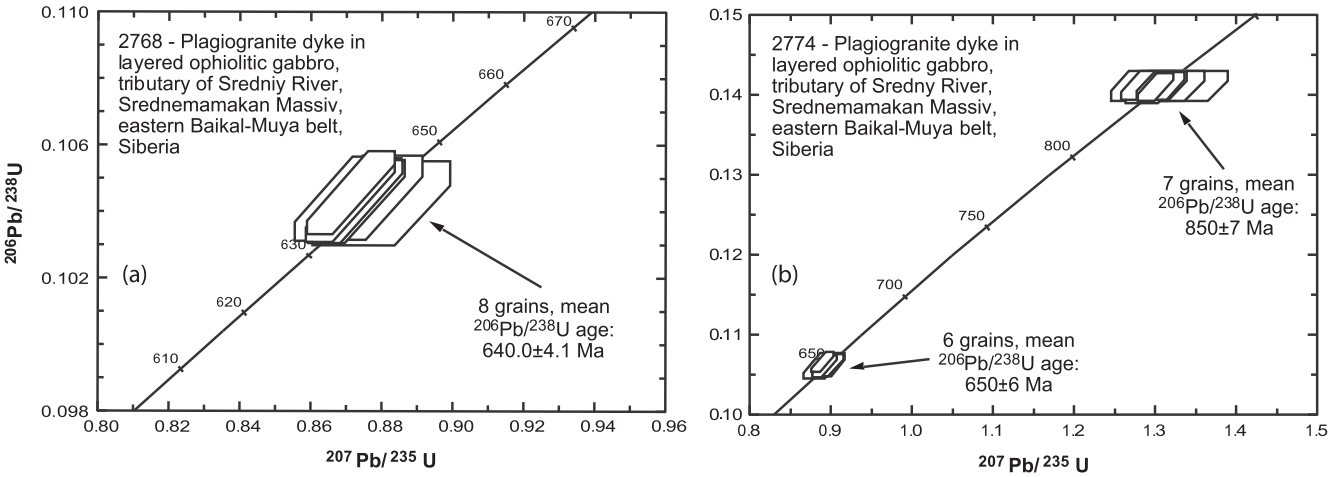

Fig. 11. Concordia diagrams showing analytical data for SHRIMP II analyses of zircon from plagiogranite dyke samples in layered gabbro of the Srednemamakan Massif, eastern Baikal–Muya belt, northern Lake Baikal area, Siberia. Data boxes for each analysis are defined by standard errors in $^{207}Pb/^{235}U$, $^{206}Pb/^{238}U$ and $^{207}Pb/^{206}Pb$. For sample locations see Table 1 and Fig. 3, for analytical data see Table 3. (a) Dyke sample 2768, (b) dyke sample 2774.

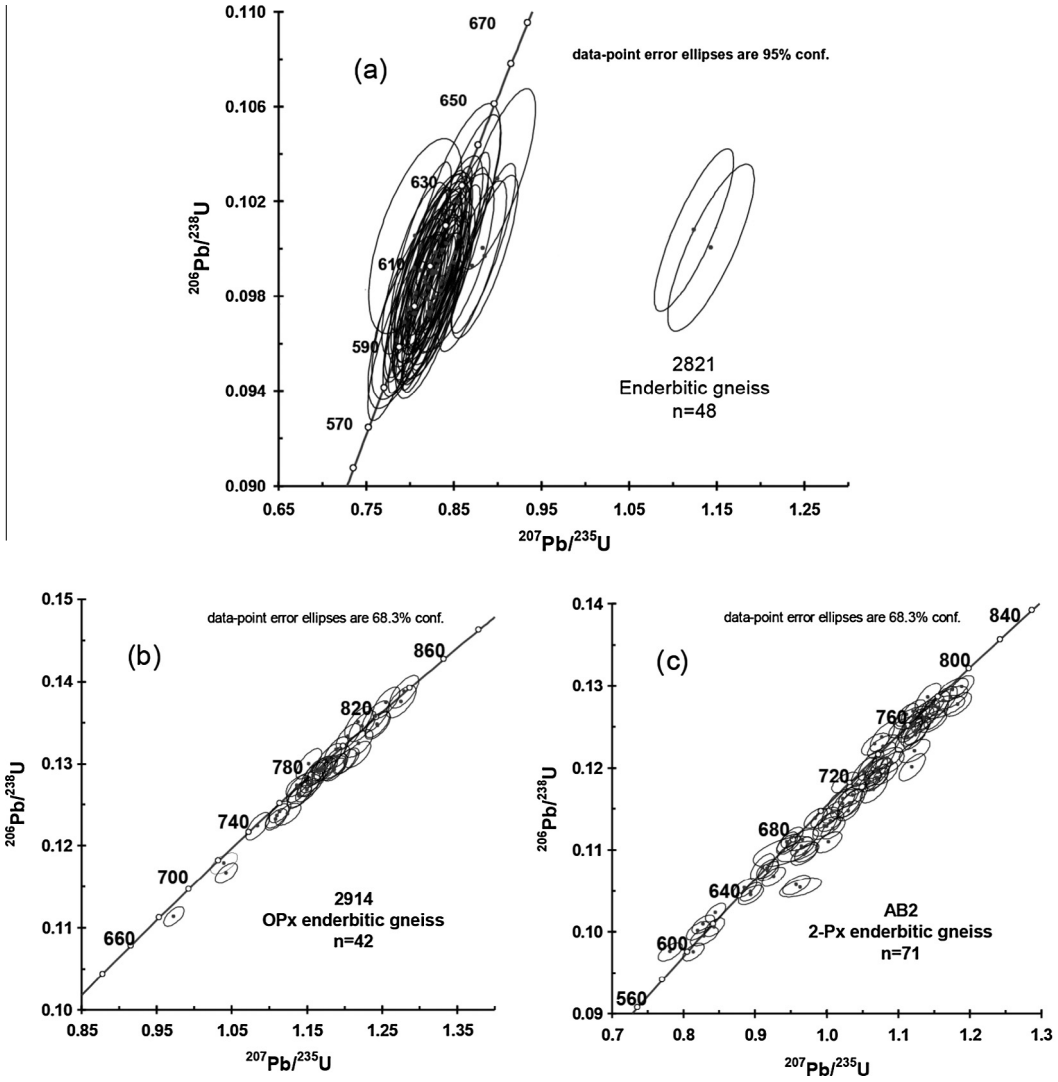

Fig. 12. Concordia diagrams showing LA-ICP-MS data for single zircons from enderbitic gneiss samples, Baikal–Muya belt, Siberia. (a) Sample 2821; (b) Sample 2914; (c) Sample AB2. Error ellipses are 1-sigma. For sample locations see Table 1 and Fig. 4, for analytical data see Table 4.

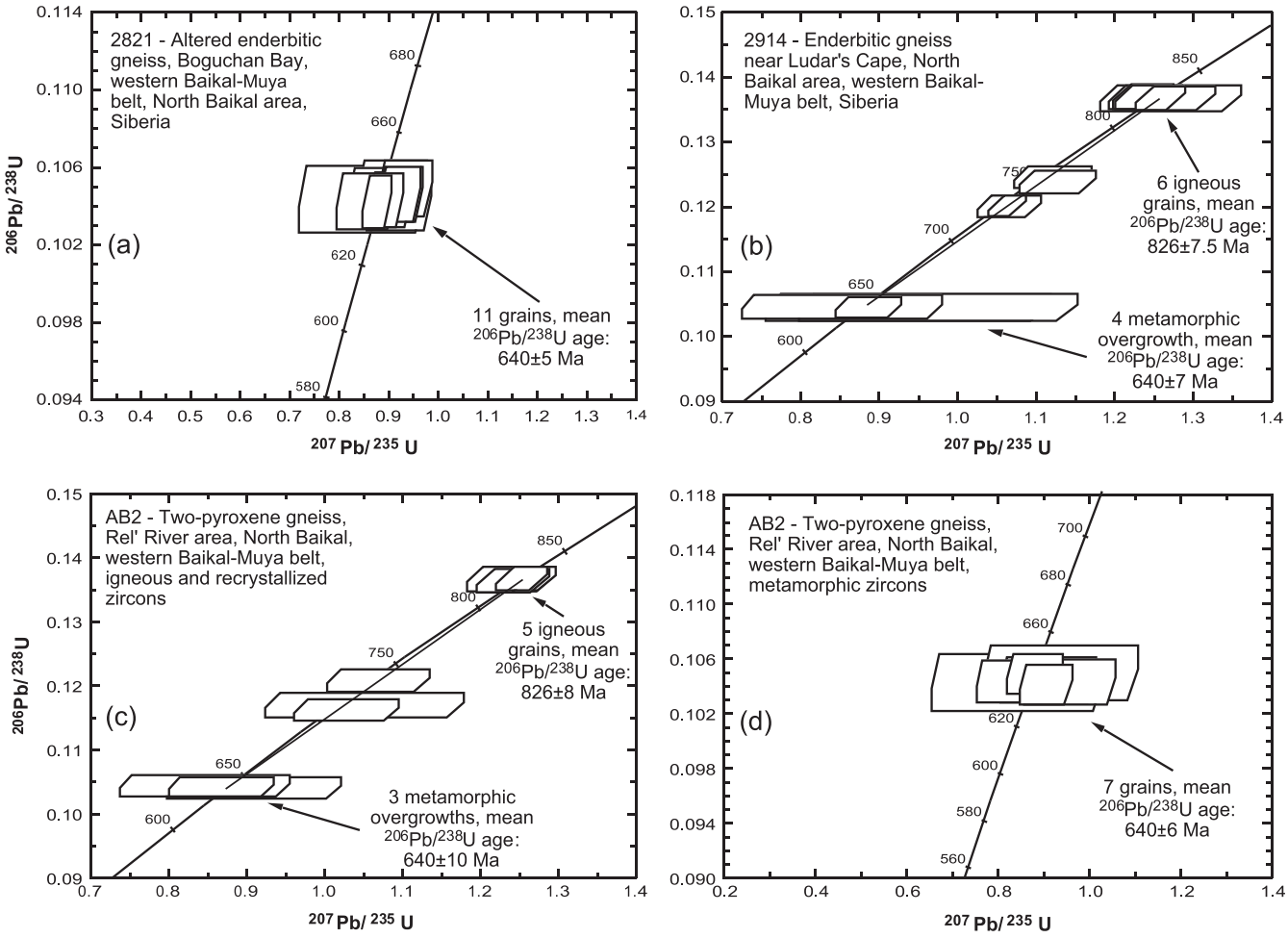

Fig. 13. Concordia diagrams showing analytical data for SHRIMP II analyses of zircon from enderbitic gneiss samples in the western Baikal–Muya belt, northern Lake Baikal area, Siberia. For sample locations see Fig. 2, for analytical data see Table 3. (a) Altered enderbitic gneiss sample 2821. (b) Enderbitic gneiss sample 2914. (c) Magmatic zircon of enderbitic gneiss sample AB2. (d) Metamorphic zircon of enderbitic gneiss sample AB2.

the primary oscillatory patterns (Fig. 10). CL-bright zones merge with narrow CL-bright rims around some grains, which are up to 30 μm thick. These CL-bright zones are identical to the CL-bright rims and are not open fractures but are completely healed fissures. The contacts between CL-bright zones and the zoned zircon are sharp (Fig. 10). The outer surfaces of the oscillatory-zoned crystals are somewhat resorbed and have cavities filled with the CL-bright zircon (Fig. 10a). These zones show no preferred orientation in relation to oscillatory zoning or crystal shape. However, in a few grains, straight CL-bright zones are nearly perpendicular to the oscillatory zoning (Fig. 10a). The amount of CL-bright zones varies from a few isolated and randomly oriented zones (Fig. 10a) to a network (Fig. 10b). The CL-bright zones extend into the rims, indicating that the CL-bright zones probably formed at the same time as the rims. These observations suggest that the magmatic grains were fractured and fragmented in a brittle manner, and these features are remarkably similar to zircon described and interpreted in a similar way by Rimša et al. (2007) from Mesoproterozoic rocks in SW Sweden.

Cracks between oscillatory zoned zircon fragments were sealed after fracturing by CL-bright zircon, and since these CL-bright zones merge with the zircon rims of likely metamorphic origin we suggest that precipitation occurred during high-grade metamorphism, presumably from hydrothermal fluids. Thus, following the interpretation of Rimša et al. (2007), we propose that the CL-bright zones cutting across the oscillatory-zoned material represent newly-formed zircon by the mechanism of crack-sealing. Rimša et al. (2007) considered hydraulic fracturing as the most likely mechanism for their fractured zircon grains and suggested that a fluid oversaturated with Zr caused sealing of the cracks. Since the crack-filled material seems to merge with the bright-CL metamorphic rims we suggest that hydrothermal precipitation during prograde metamorphism and deformation seems a likely mechanism for the formation of the CL-bright zircon in the cracks.

6. Zircon geochronology

One reason for undertaking this study was that most zircon analyses obtained on the high-grade gneisses by laser ablation ICP-MS were inconclusive since many data points appeared to be concordant and formed long arrays on Concordia that did not permit to either determine reliable igneous or metamorphic ages. Furthermore, these analyses were performed without CL imagery, and it was thus impossible to relate the data to specific parts of the analyzed zircons. Below we compare and contrast the LA-ICP-MS data with the results obtained from SHRIMP analyses based on CL images.

The location of the dated rocks are shown in Fig. 2, and the analytical data are shown in Table 3 (SHRIMP results) and Table 4 (LA-ICP-MS results). The analytical procedures are described in the Appendix A.

6.1. Plagiogranite ages

Zircons from two samples of plagiogranite were only analyzed on the SHRIMP II instrument. Eight grains of the magmatic zircon population of plagiogranite dyke sample 2768 from the Sredne–Mamakan massif in the eastern Baikal–Muya belt provided identical concordant data (Table 3) with a mean $^{206}Pb/^{238}U$ age of 640.0 ± 4.1 Ma (Fig. 11a). We interpret this to reflect the time of plagiogranite crystallization and, by implication, the age of the Neoproterozoic Mamakan ophiolite.

The magmatic zircon population of plagiogranite dyke sample 2774 from the same ophiolitic gabbro is isotopically more complex although this is not obvious from their CL-images. Six grains yielded concordant results (Table 2), as in sample 2768, with a mean $^{206}Pb/^{238}U$ age of 650 ± 6 Ma (Fig. 9b). Although apparently some 10 Ma older than dyke sample 2768, the results are similar, within error, and we therefore suggest an age of ca. 645 Ma as the most likely time of dyke emplacement and ophiolite formation. Seven additional grains from sample 2774, morphologically indistinguishable from the above grains, also yielded concordant results (Table 3) that are considerably older than the 650 Ma population and yielded a mean $^{206}Pb/^{238}U$ age of 850 ± 7 Ma (Fig. 11b). We consider these to be xenocrysts, but their origin is not known. We discuss the problem of zircon xenocrysts in ophiolites below.

6.2. Ages of enderbitic gneisses from the western part of the Baikal–Muya belt

Forty-eight zircon grains of enderbitic gneiss sample 2821 were analyzed by LA-ICP-MS (Table 4) of which 46 data points form a well-defined concordant cluster in the concordia diagram with a mean $^{206}Pb/^{238}U$ age of 615 Ma (Fig. 12a). Two analyses have similar $^{206}Pb/^{238}U$ ratios as this cluster but much higher $^{207}Pb/^{235}U$ and $^{207}Pb/^{206}Pb$ ratios that is likely to be the result of insufficient common Pb correction. We do not interpret these grains to be old xenocrysts, because the SHRIMP analyses reported below did not yield old ages, and the CL images do not show any core-rim relationships. Therefore, the two anomalous analyses are discarded.

Eleven magmatic grains were analyzed by SHRIMP from altered enderbite sample 2821, and all data are concordant (Table 3) with a mean $^{206}Pb/^{238}U$ age of 640 ± 5 Ma (Fig. 13a). Since the magmatic nature of these grains is not in doubt (see Fig. 9d), we interpret this age to reflect the time of emplacement of the enderbite protolith. This mean age is slightly higher than the age obtained by LA-ICP-MS but overlaps with the cluster in Fig. 12a.

The zircon population of enderbitic gneiss sample 2914 is more complex since metamorphic overgrowth and crack-formation and -sealing was observed (Fig. 9e–g). This information was not available for the LA-ICP-MS analyses, and these data constitute a broad swath along concordia between ca. 840 and 680 Ma with some data points apparently concordant and some somewhat discordant (Fig. 12a). This distribution is reminiscent of the data shown in Fig. 8 and strongly suggests that the analyses reflect two end-member components, namely an igneous crystallization event at ca. 800 Ma a Pb-loss and recrystallization event at ca. 600 Ma. Such an interpretation is confirmed by the CL images and the SHRIMP data discussed below.

Six magmatic grains were analyzed on SHRIMP II and yielded concordant results (Table 3) with a mean $^{206}Pb/^{238}U$ age of 826 ± 7.5 Ma (Fig. 13b). Four additional magmatic grains produced significantly younger apparent $^{206}Pb/^{238}U$ ages, and their error symbols may suggest that they are concordant (Fig. 13b). Four analyses of the highly luminescent and low-U metamorphic rims yielded concordant $^{206}Pb/^{238}U$ ages with large $^{207}Pb/^{235}U$ errors due to low count rates (Table 3), and the mean $^{206}Pb/^{238}U$ age is 640 ± 7 Ma (Fig. 13b). We interpret this to reflect zircon growth close to the peak of high-grade metamorphism. The four igneous grains plotting between the 826 Ma population and the data for metamorphic overgrowth are considered to have lost radiogenic Pb during high-grade metamorphism or represent recrystallized material. Therefore, these analyses, although apparently concordant as seen in the concordia diagram are, in fact, discordant and plot on a line close to Concordia and connecting the magmatic and metamorphic zircon populations (Fig. 13b). Thus, the most likely explanation of the zircon analyses is that the enderbite protolith crystallized at 826 ± 7.5 Ma and experienced the peak of granulite-metamorphism at 640 ± 7 Ma. The LA-ICP-MS analyses are fully compatible with this interpretation.

Finally, the zircon data of two-pyroxene enderbitic gneiss sample AB2 are very similar to those of 2914. As in the previous case, seventy-one LA-ICP-MS analyses form a broad swath of concordant and near-concordant data points between ca. 800 and 600 Ma in the concordia diagram (Fig. 12c), again pointing to a two-component system with igneous crystallization at ca. 800 Ma and an ill-defined metamorphic overprint ca. 600 Ma.

Five igneous grains analyzed on SHRIMP II yielded concordant results (Table 3) with a mean $^{206}Pb/^{238}U$ age of 826 ± 8 Ma (Fig. 13c) that is identical to the magmatic zircon ages of sample 2914 and is interpreted to reflect the time of enderbite protolith crystallization. Three low-U metamorphic rims have identical and concordant $^{206}Pb/^{238}U$ ages with a mean of 640 ± 10 Ma, also

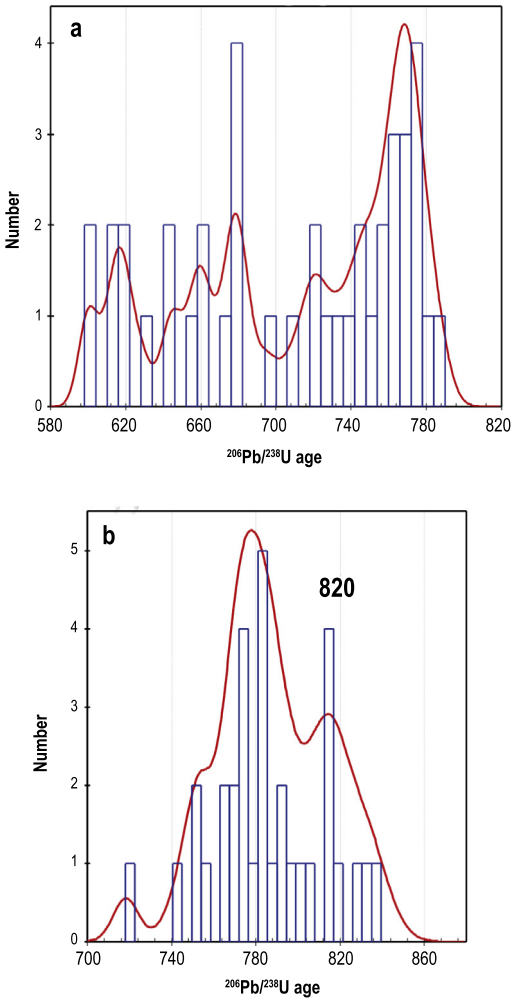

Fig. 14. Histograms showing distribution of apparent $^{206}Pb/^{238}Pb$ ages from LA-ICP-MS zircon analyses; for data see Table 4. (a) Apparent age distribution in enderbitic gneiss sample AB2. (b) Apparent age distribution in enderbitic gneiss sample 2914.

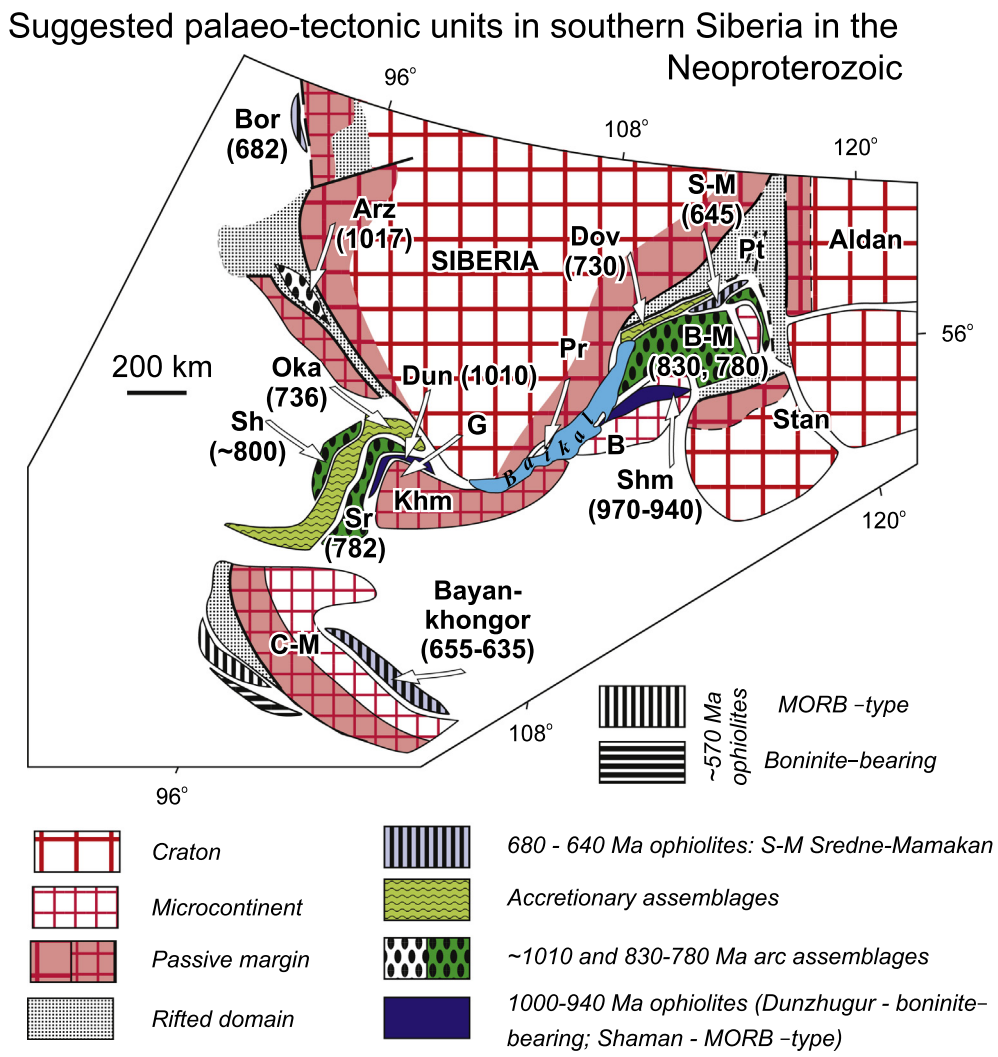

Fig. 15. Suggested palaeotectonic units (present reference frame), reconstructed along the southern margin of the Siberian craton in the Neoproterozoic (modified after Khain et al., 2003). For explanation see text. 680–640 Ma ophiolites: Bor = Borisikha Massif (Kuzmichev et al., 2008); Bayankhongor zone (Jian et al., 2010; Terenteva et al., 2008); S–M = Sredne–Mamakan (this study). Accretionary assemblages, intruded by Oka sills (Kuzmichev et al., 2007) and Dov = Dovyren sill (Ariskin et al., 2013). ~1010 and 830–780 Ma arc assemblages: Arz = Arzybey (Turkina et al., 2004) and Sh = Shishkhid (Kuzmichev et al., 2005); Sr = Sarkhoy (Kuzmichev and Larionov, 2011); B–M = Baikal–Muya (Izokh et al., 1998; Rytsk et al., 2001a,b; this study). 1000–940 Ma ophiolites: Dun = Dunzhugur (Khain et al., 2002; Kuzmichev and Larionov, 2013); Shm = Shaman (Nekrasov et al., 2007; Gordienko et al., 2009, 2010). ~570 Ma ophiolites (Khain et al., 2003; Jian et al., 2014). Reworked continental blocks with early Precambrian cores: C-M = Central Mongolia, 2.65 Ga (Kozakov et al., 2007); G = Gargan antiform (2.66 Ga (Kovach et al., 2004)) within Khamardaban (Khm) block; B = Barguzin, 2.67 Ga (Ruzhentsev et al., 2012); numbers (in Ga) are ages of the oldest dated rocks in the metamorphic complexes.

similar to sample 2914 (Table 3, Fig. 13c). Three analyses of igneous grains plot between these two concordant groups and, as in sample 2914, are interpreted to have lost radiogenic Pb or are recrystallized, and plot on a discordia line connecting the 826 and 640 Ma age groups (Fig. 13c). Seven ball-round metamorphic grains also produced concordant analyses (Table 3) with a mean $^{206}Pb/^{238}U$ age of 640 ± 6 Ma (Fig. 13d), identical to the metamorphic rims on the igneous zircon and likewise reflecting crystallization at or near the peak of granulite-facies metamorphism.

7. Discussion and conclusions

This zircon dating exercise produced unambiguous results that, combined with the interpretation of CL-images, makes it possible to assign the obtained ages to distinct igneous and metamorphic events. The highly variable results previously obtained by LA-ICP-MS on single zircon from the same samples, but without previous CL-identification, can be now be explained as follows.

LA-ICP-MS analyses of grains from enderbite sample AB2 vary between 570 and 790 Ma (Figs. 12c, 14a) that resulted from variable $^{206}Pb/^{238}U$ ratios due to Pb-loss at 640 Ma and mixing between the 826 Ma magmatic and 640 Ma metamorphic components. The few grains with apparent $^{206}Pb/^{238}U$ ages <640 Ma (Figs. 12c, 14) likely lost Pb after 640 Ma. Likewise, LA-ICP-MS analyses of grains from enderbite sample 2914 yielded apparent $^{206}Pb/^{238}U$ ages between ca. 678 and 840 Ma (Figs. 12b, 14b) and this is likely the result of Pb-loss at about 640 Ma and mixing between the 826 Ma magmatic and 640 Ma metamorphic components. In summary, the apparent spread in $^{206}Pb/^{238}U$ ratios resulting from LA-ICP-MS analyses is due to isotopic mixing of igneous and metamorphic components, and these data do not provide geologically meaningful results.

The implications of the ages reported in this study for the evolution of the Neoproterotoic to early Palaeozoic terrane of the Baikalian mountain area can be summarized as follows. Our geochronological data and previously published ages for Neoproterozoic igneous rocks of the Barguzin Block and

Baikal–Muya belt define two age groups at 830–780 and 650–640 Ma. We now compare these groups with ages for arc-related assemblages in eastern Sayan and northwestern Mongolia and propose the following palaeotectonic reconstruction.

The older group of 830–780 Ma includes the age of igneous zircon cores from the North Baikal granulites (western segment of the Baikal–Muya belt) at 826 Ma (this study), and ages of an arc-related metavolcanic rock (824 ± 2 Ma, Rytsk et al., 2001a,b) and gabbro (835 ± 12, Izokh et al., 1998) from the eastern segment of the Baikal–Muya belt. Arc-related felsic volcanic rocks in northwestern Mongolia and eastern Sayan formed at 800–780 Ma and are represented by the Shishkhid and Sarkhoy volcanic sequences (~800 Ma, Kuzmichev et al., 2005, and 782 ± 11, Kuzmichev and Larionov, 2011, respectively). Arc-related tonalites (785 ± 11 Ma, Kuzmichev et al., 2001) in eastern Sayan intruded rocks of the early Precambrian Gargan Block. A sample of the Muya granite-gneisses in the Baikal–Muya belt yielded an age of ~785 Ma (Rytsk et al., 2001a,b).

From these data we can reconstruct a large arc system in the Baikal–Muya belt and the eastern Sayan – northwestern Mongolia region for the time interval 780–830 Ma, represented by volcanic rocks in the Sayan-Mongolia area and by magmatic and metamorphic rocks or their igneous protholiths (this work) in the Baikal–Muya belt (Fig. 15). The relicts of a latest Mesoproterozoic to early Neoproterozoic oceanic archipelago, represented by the Dunzhugur ophiolite (Khain et al., 2002; Kuzmichev and Larionov, 2013) and mafic rocks recognized in the Barguzin Block (939–918 Ma, Ruzhentsev et al., 2010; Gordienko et al., 2009) trace the southern and eastern sides of this reconstructed arc-related Sarkhoy-Baikal–Muya belt.

The younger age group of 650–640 Ma leads to the following scenario. The early phase of collision between the above >780 Ma archipelago-type palaeostucture and the Siberian craton is marked by eclogites (631 ± 17 Ma, Shatsky et al., 2012) and granulites (~640 Ma, this study) in the Muya block and the North Baikal segment of the Baikal–Muya belt. This probably reflects transpressional and transtensional settings along the boundary of this evolving continental fragment. Ophiolite fragments are probably the relicts of an arc-related basin that existed prior to an early collision event at 650–640 ago (this study and data from harzburgites of the Chaya Massif, dated at ca. 640 Ma, Amelin et al., 1997).

The second phase of collision in the time interval 470–498 Ma is recognized in the Priolkhonye segment at the boundary between the heterogeneous Barguzin Block and the Siberian craton (Gladkochub et al., 2010). This collision was probably related to the closure of a basin that existed at about 530 Ma ago along the southern present-day boundary of the Barguzin Block (Ruzhentsev et al., 2010). In summary, the Baikalian Mountains as well as the Sayan-Mongolian area are segments of a circum-Siberian belt, including latest Mesoproterozoic to late Neoproterozoic ophiolites, related to the evolution of island-arc related basins, and relicts of a large 830–800 Ma arc system (Fig. 15).

Acknowledgements

Chun Yang of the Beijing SHRIMP Centre prepared a perfect zircon mount, and Ning Li and Liqin Zhou provided the zircon CL images. We also acknowledge E. Yu. Rytsk, St. Petersburg, for his help in conducting this study and for fruitful discussions during fieldwork. This is part of a collaborative study between Mainz and Munich Universities and The University of Hong Kong, funded jointly by the German Exchange Service (DAAD) and the Hong Kong Research Council. This research was also supported by the Russian Foundation for Basic Research (Project Nos. 11-05-01052, 12-05-31246), and fieldwork in the North Baikal area was supported by the (Russian) Foundation for Development of Domestic Geology. This is a contribution to IGCP Project 592 (Continental Construction in Central Asia).

Appendix A. – Analytical techniques

A.1. LA-ICP-MS

Isotopic measurements were performed in the Laboratory of Isotope Geochemistry and Geochronology of the Vernadsky Institute of Geochemistry and Analytical Chemistry, Russian Academy of Sciences, Moscow, using an Element-XR (Thermo-Finnigan) ICP-MS equipped with a New Wave UP-213 laser. The analytical techniques were similar to those described in Jackson et al. (2004).

Zircons were concentrated by conventional techniques and then washed in a mixture of nitric and hydrofluoric acids in an ultrasonic bath for 30 min. to remove possible natural and laboratory contaminants. After rinsing in distilled water the grains were dried, and representative grains were handpicked under a binocular microscope and mounted on double-sided tape and cast into a 25 mm epoxy mount. The mount was then polished to expose the zircon interiors and again washed in 5% nitric acid and distilled water prior to analysis. Details of the chamber containing the zircon and standard mounts as well as operating conditions are described in Kostitsyn and Anosova (2013). The laser spot size was 30 μm, the pulse rate was 4 Hz and the enery density at the spot was 10–15 J/cm^2. Zircon standards used were GJ (Jackson et al., 2004) and 91500 (Wiedenbeck et al., 1995).

A.2. SHRIMP zircon dating

Zircons were hand-picked from concentrates prepared in the Institute of Precambrian Geology and Geochronology, Russian Academy of Sciences (RAS), St. Petersburg (samples 2768, 2774) and in the Geological Institute, RAS, in Moscow (samples 2821, AB2, 2914) and mounted in epoxy resin together with chips of the standard M257 (Nasdala et al., 2008) for SHRIMP analyses. The mount was ground down and polished so that the zircon cores were exposed, and zircons were photographed under cathodoluminescence (CL) to enable easy and best location of suitable spots for SHRIMP analysis. CL imaging was done on a 305 Hitachi SEM S-3000N equipped with a Gatan ChromaCL detector and a DigiSan II data306 recorder in the Beijing SHRIMP Center. Operating conditions were 9 kV, 99 μA.

Isotopic analyses were performed on the Beijing SHRIMP II ion microprobe whose instrumental characteristics were described by De Laeter and Kennedy (1998). The analytical procedures are outlined in Compston et al. (1992), Claoué-Long et al. (1995), Nelson (1997) and Williams (1998). Prior to each analysis, the surface of the analysis site was cleaned by rastering of the primary beam for 2 min. to reduce or eliminate surface common Pb. The reduced $^{206}Pb/^{238}U$ ratios were normalized to 0.09101, which is equivalent to the adopted age of 561.3 Ma for standard zircon M257 (Nasdala et al., 2008). Pb/U ratios in the unknown samples were corrected using the ln(Pb/U)/ln(UO/U) relationship as measured in M257 and as outlined in Compston et al. (1984) and Nelson (1997). The 1σ error in the ratio $^{206}Pb/^{238}U$ during analysis of all standard zircons during this study was 1.3%. Primary beam intensity was 4.2 nA, and a Köhler aperture of 100 μm diameter was used, giving a slightly elliptical spot size of about 30 μm. Peak resolution was 4920 (at 1% peak height) on mass ^{254}UO of the standard, enabling clear separation of the ^{208}Pb-peak from the HfO peak. Analyses of samples and standards were alternated to allow assessment of Pb^+/U^+ discrimination.

Raw data reduction and error assessment followed the method described by Nelson (1997). Common Pb corrections have been applied using the ^{204}Pb-correction method and assuming the isotopic composition of Broken Hill, because common Pb is thought to be surface-related (Kinny, 1986). The analytical data are presented in Table 2. Errors given on individual analyses are based on counting statistics and are at the 1σ level and include the uncertainty of the standard added in quadrature. Errors for pooled analyses are at 2σ. The ages and errors were calculated for mean ^{206}Pb/^{238}U ratios, including the calibration error on 12 standards measured during the analytical session.

References

Amelin, Y.V., Ritsk, E.Y., Neymark, L.A., 1997. Effects of interaction between ultramafic tectonite and mafic magma on Nd–Pb–Sr isotopic systems in the Neoproterozoic Chaya Massif, Baikal–Muya ophiolite belt. Earth Planet. Sci. Lett. 148, 299–316.

Amelin, Yu.V., Rytsk, E.Yu., Krymskii, R.Sh., Neymark, L.A., Skublov, S.G., 2000. Vendian age of enderbites from a granulite complex of the Baikal–Muya ophiolite belt, northern Baikal region: U–Pb and Sm–Nd isotope evidence. Transactions (Doklady) Russian Academy of Sciences. Earth Sci. 371, 455–457 (in Russian).

Anders, E., Grevesse, N., 1989. Abundances of elements: meteoritic and solar. Geochim. Cosmochim. Acta 53, 197–214.

Ariskin, A.A., Kostitsyn, Yu.A., Nikolaev, G.S., Konnikov, E.G., Danyushevsky, L.V., Meffre, S., McNeill, A., Kislov, E.V., Orsoev, D.A., 2013. Geochronology of the Dovyren intrusive complex, northwestern Baikal area, Russia, in the Neoproterozoic. Geochem. Int. 51, 859–875.

Chumakov, N.M., Pokrovskii, B.G., Melezhik, V.A., 2007. Geological history of the Late Precambrian Patom Supergroup (Central Siberia). Dokl. Earth Sci. 413, 343–346.

Claoué-Long, J.C., Compston, W., Roberts, J., Fanning, C.M., 1995. Two Carboniferous ages: a comparison of SHRIMP zircon dating with conventional zircon ages and ^{40}Ar/^{39}Ar analyses. Soc. Sediment. Geol. Special Publ. 54, 3–21.

Compston, W., Williams, I.S., Myer, C., 1984. U–Pb geochronology of zircons from Lunar Breccia 73217 using a sensitive high mass-resolution ion-microprobe. J. Geophys. Res. 89 (Suppl.), B525–B534.

Compston, W., Williams, I.S., Kirschvink, J.L., Zhang, Z., Ma, G., 1992. Zircon U–Pb ages for the early Cambrian time scale. J. Geol. Soc. London 149, 171–184.

Connelly, J.N., 2001. Degree of preservation of igneous zonation in zircon as a signpost for concordancy in U–Pb geochronology. Chem. Geol. 172, 25–39.

Corfu, F., 2007. Multistage metamorphic evolution and nature of the amphibolite-granulite facies transition in Lofoten-Vesterålen, Norway, revealed by U–Pb in accessory minerals. Chem. Geol. 241, 108–128.

Corfu, F., 2013. A century of U–Pb geochronology. The long quest towards concordance. Geol. Soc. Am. Bull. 125, 33–47.

Corfu, F., Heaman, L.M., Rogers, G., 1994. Polymetamorphic evolution of the Lewisian complex, NW Scotland, as recorded by U–Pb isotopic compositions of zircon, titanite and rutile. Contrib. Miner. Petrol. 117, 215–228.

De Laeter, J.R., Kennedy, A.K., 1998. A double focusing mass spectrometer for geochronology. Int. J. Mass Spectrom. 178, 43–50.

Dong, C.Y., Wan, Y.S., Xu, Z.Y., Liu, D.Y., Yang, Z.S., Ma, M.Z., Xie, H.Q., 2013. Khondalites of the late Paleoproterozoic in the Daqingshan area, North China Craton: SHRIMP zircon U–Pb dating. Sci. China, Ser. D 56, 115–125.

Fedotova, A.A., Razumovskiy, A.A., Khain, E.V., Anosova, M.O., Orlova, A.V., 2014. Late neoproterozoic igneous complexes of the western Baikal–Muya belt: formation stages. Geotectonics 48, 292–312.

Flowers, R.M., Schmitt, A.K., Grove, M., 2010. Decoupling of U–Pb dates from chemical and crystallographic domains in granulite facies zircon. Chem. Geol. 270, 20–30.

Geisler, T., Schaltegger, U., Tomaschek, F., 2007. Re-equilibration of zircon in aqueous fluids and melts. Elements 3, 43–50.

Gladkochub, D.P., Donskaya, T.V., Wingate, M.T.D., Poller, U., Kröner, A., Fedorovsky, V.S., Mazukabzov, A.M., Todt, W., Pisarevsky, S.A., 2008. Petrology, geochronology, and tectonic implications of c. 500 Ma metamorphic and igneous rocks along the northern margin of the Central Asian Orogen (Olkhon terrane, Lake Baikal, Siberia). J. Geol. Soc. Lond. 165, 235–246.

Gladkochub, D.P., Donskaya, T.V., Fedorovsky, V.S., Mazukabzov, A.M., Larionov, A.N., Sergeev, S.A., 2010. The Olkhon metamorphic terrane in the Baikal region: an early Paleozoic collage of Neoproterozoic active margin fragments. Russ. Geol. Geophys. 51, 447–460.

Gladkochub, D.P., Stanevich, A.M., Mazukabzov, A.M., Donskaya, T.V., Pisarevskii, S.A., Nicoll, G., Motova, Z.L., Kornilova, T.A., 2013. Early evolution of the Paleoasian ocean: LA-ICP-MS dating of detrital zircon from Late Precambrian sequences on the southern flank of the Siberian craton. Russ. Geol. Geophys. 54, 1150–1163.

Gordienko, I.V., Bulgatov, A.N., Lastochkin, N.I., Sitnikova, V.S., 2009. Composition and U–Pb Isotopic Age determinations (SHRIMP II) of the ophiolitic assemblage from the shaman paleospreading zone and the conditions of its formation (North Transbaikalia). Dokl. Earth Sci. 429A, 1420–1425.

Gordienko, I.V., Bulgatov, A.N., Minina, O.R., Klimuk, V.S., Vetluzhskikh, L.I., Sitnikova, V.S., Goneger, T.A., Ruzhentsev, S.V., Nekrasov, G.E., Metelkin, D.V., Lepekhina, E.N., Lastochkin, N.I., 2010. The late Riphean-Paleozoic history of the Uda-Vitim island arc system of the Transbaikal sector of the Paleoasian ocean. Russ. Geol. Geophys. 51, 461–481.

Gordienko, I.V., Kovach, V.P., Elbaev, A.L., Kotov, A.B., Sal'nikova, E.B., Reznitskii, L.Z., Yakovleva, S.Z., Anisimova, I.V., 2012. Collisional granitoids of the Dzhida zone of the Central Asian Fold belt, Southwestern Transbaikalia: age and conditions of the formation. Petrology 20, 40–58.

Izokh, A.E., Gibsher, A.S., Zhuravlev, D.Z., Balykin, P.A., 1998. Sm–Nd data on the age of ultramafic-mafic massifs, eastern branch of the Baikal–Muya ophiolite belt. Doklady Akademi Nauk 360, 88–92 (in Russian).

Jackson, S.E., Pearson, N.J., Griffin, W.L., Belousova, E.A., 2004. The application of laser ablation inductively-coupled plasma-mass spectrometry to in-situ zircon geochronology. Chem. Geol. 211, 47–69.

Jian, Ping, Kröner, Alfred, Windley, Brinan F., Shi, Yuruo, Zhang, Fuqin, LMiao, Lucheng, Tomurhuu, Dondov, Zhang, Wei, Liu, Dunyi, 2010. Zircon ages of the Bayankhongor ophiolite mélange and associated rocks: time constraints on Neoproterozoic to Cambrian accretionary and collisional orogenesis in Central Mongolia. Precambrian Res. 177, 162–180.

Jian, P., Kröner, A., Jahn, B.-M., Windley, B.F., Shi, Y., Zhang, W., Zhang, F., Miao, L., Tomurhuu, D., Liu, D., 2014. Zircon dating of Neoproterozoic and Cambrian ophiolites in West Mongolia and implications for the timing of orogenic processes in the central part of the Central Asian Orogenic Belt. Earth Sci. Rev. 133, 62–93.

Khain, E.V., Bibikova, E.V., Kroöner, A., Zhuravlev, D.Z., Sklyarov, E.V., Fedotova, A.A., Kravchenko-Berezhnoy, I.R., 2002. The most ancient ophiolite of the Central Asian fold belt: U–Pb and Pb–Pb zircon ages for the Dunzhugur Complex, Eastern Sayan, Siberia, and geodynamic implications. Earth Planet. Sci. Lett. 199, 311–325.

Khain, E.V., Bibikova, E.V., Salnikova, E.B., Kröner, A., Gibsher, A.S., Didenko, A.N., Degtyarev, K.E., Fedotova, A.A., 2003. The Palaeo-Asian ocean in the neoproterozoic and early palaeozoic: new geochronologic data and palaeotectonic reconstructions. Precambr. Res. 122, 329–358.

Khain, E.V., Fedotova, A.A., Nekrasov, G.E., Orlova, A.V., Razumovskiy, 2014. Rock associations – indicators of the origin of the Baikal–Muya belt. In: Sklyarov, E.V. (Ed.), Geodynamic Evolution of the Lithosphere of the Central Asian Foldbelt (from Ocean to Continents). Institute of the Earth's Crust, Irkutsk, Russia, pp. 320–322.

Khain, V.E., Gusev, G.S., Khain, E.V., Vernikovsky, V.A., Volobuyev, M.I., 1997. Circum-Siberian Neoproterozoic ophiolite belt. Ofioliti 22, 195–200.

Khudoley, A.K., Rainbird, R.H., Stern, R.A., Kropachev, A.P., Heaman, L.M., Zanin, A.M., Podkovyrov, V.N., Belova, V.N., Sukhorukov, V.I., 2001. Sedimentary evolution of the Riphean–Vendian basin of southeastern Siberia. Precambr. Res. 111, 129–163.

Kinny, P.D., 1986. 3820 Ma zircons from a tonalitic Amitsoq gneiss in the Godthab district of southern West Greenland. Earth Planet. Sci. Lett. 79, 337–347.

Konnikov, E.G., Gibsher, A.S., Izokh, A.E., Sklyarov, E.V., Khain, E.V., 1994. Late-Proterozoic evolution of the northern segment of the Paleoasian Ocean: new radiological and geochemical data. Russ. Geol. Geophys. 35, 152–168.

Konnikov, E.G., Tsygankov, A.A., Vrublevskaya, T.T., 1999. The Baikal–Muya Volcano-Plutonic Belt: Structures, Substance and Geodynamics. GEOS Publishing House, Moscow, 163p. (in Russian).

Kooijman, E., Upadhyay, D., Mezger, K., Raith, M.M., Berndt, J., Srikantappa, C., 2011. Response of the U–PB chronometer and trace elements in zircon to untrahigh-temperature metamorphism: the Kadavur anorthosite complex, southern India. Chem. Geol. 20, 177–188.

Kostitsyn, Yu.A., Anosova, M.O., 2013. U–Pb age of extrusive rocks in the Uxichan Caldera, Sredinnyi Range, Kamchatka: application of laser ablation in dating young zircons. Geochem. Int. 51, 155–163.

Kovach, V.P., Matukov, D.I., Berezhnaya, N.G., Kotov, A.B., Levitsky, V.I., Barash, I.G., Kozakov, I.K., Levsky, L.K., Sergeev, S.A., 2004. SHRIMP zircon age of the Gargan block tonalites – find early Precambrian basement of the Tuvino-Mongolian microcontinent, Central Asia Mobile Belt. In: 32th International Geological Congress, Abstracts, 284–48, 1263.

Kovach, V.P., Sal'nikova, E.B., Rytsk, E.Yu., Yarmolyuk, V.V., Kotov, A.B., Anisimova, I.V., Yakovleva, S.Z., Fedoseenko, A.M., Plotkina Yu, V., 2012. The time length of formation of the Angara–Vitim Batholite: Results of U–Pb geochronological studies. Dokl. Earth Sci. 444, 553–558.

Kozakov, I.K., Sal'nikova, E.B., Wang, T., Didenko, A.N., Plotkina, Y.V., Podkovyrov, V.N., 2007. Early Precambrian crystalline complexes of the central Asian microcontinent: age, sources, tectonic position. Stratigr. Geol. Correl. 15, 121–140.

Kröner, A. (Ed.), 2015. The Central Asian Orogenic Belt. Borntraeger Science Publishers, Stuttgart, Germany, 313p.

Kröner, A., Kovach, V., Belousova, E., Hegner, E., Armstrong, R., Dolgopolova, A., Seltmann, R., Alexeiev, D.V., Hoffmann, J.E., Wong, J., Sun, M., Cai, K., Wang, T., Tong, Y., Wilde, S.A., Degtyarev, K.E., Rytsk, E., 2014. Reassessment of continental growth during the accretionary history of the Central Asian Orogenic Belt. Gondwana Res. 25, 103–125.

Kröner, A., O'Brien, P.J., Nemchin, A.A., Pidgeon, R.T., 2000. Zircon ages for high-pressure granulites from South Bohemia, Czech Republic, and their connection to Carboniferous high temperature processes. Contrib. Miner. Petrol. 138, 127–142.

Kröner, A., Rojas-Agramonte, Y., Kehelpannala, K.V.W., Zack, T., Hegner, E., Wong, J., Barth, M., 2013. Age, Nd–Hf isotopes, and geochemistry of the Vijayan complex

of eastern and southern Sri Lanka: a Grenville-age magmatic arc of unknown derivation. Precambr. Res. 234, 288–321.
Kröner, A., Santosh, M., Hegner, E., Shaji, E., Geng, H., Wong, J., Xie, X., Wan, Y., Shang, C.K., Liu, D., Sun, M., Nanda-Kumar, V., 2015. Palaeoproterozoic ancestry of Pan-African high-grade granitoids in southernmost India: implications for Gondwana reconstructions. Gondwana Res. 27, 1–37.
Kuzmichev, A.B., Bibikova, E.V., Zhuravlev, D.Z., 2001. Neoproterozoic (800 Ma) orogeny in the Tuva-Mongolian Massif (Siberia): island arc-continent collision at the northeast Rodinia margin. Precambr. Res. 110, 109–126.
Kuzmichev, A., Kröner, A., Hegner, E., Liu, D.Y., Wan, Y.S., 2005. The Shishkhid ophiolite, northern Mongolia: a key to the reconstruction of a Neoproterozoic island–arc system in central Asia. Precambr. Res. 138, 125–150.
Kuzmichev, A., Sklyarov, E., Postnikov, A., Bibikova, E., 2007. The Oka Belt (Southern Siberia and Northern Mongolia): a Neoproterozoic analog of the Japanese Shimanto Belt? Island Arc 16, 224–242.
Kuzmichev, A.B., Paderin, I.P., Antonov, A.V., 2008. Late Riphean Borisikha ophiolite (Yenisei Ridge): U–Pb zircon age and tectonic setting. Russ. Geol. Geophys. 49, 883–893.
Kuzmichev, A.B., Larionov, A.N., 2011. The Sarkhoi group in East Sayan: Neoproterozoic (~770–800 Ma) volcanic belt of the Andean type. Russ. Geol. Geophys. 52, 685–700.
Kuzmichev, A.B., Larionov, A.N., 2013. Neoproterozoic island arcs in East Sayan: duration of magmatism (from U–Pb zircon dating of volcanic clastics). Russ. Geol. Geophys. 54, 34–43.
Kuz'min, M.I., Yarmolyuk, V.V., Spiridonov, A.I., Nemerov, V.K., Ivanov, A.I., Mitrofanov, G.L., 2006. Geodynamic setting of gold ored of the Neoproterozoic Bodaibo Trough. Dokl. Earth Sci. 407, 397–400.
Ledneva, G.V., Bazylev, B.A., Lebedev, V.V., Kononkova, N.N., Ishiwatari, A., 2012. U–Pb zircon age of gabbroids of the Ust'-Belaya mafic–ultramafic massif (Chukotka) and its interpretation. Geochem. Int. 50, 44–53.
Ma, M., Wan, Y., Santosh, M., Xu, Z., Xie, H., Dong, C., Liu, D., Guo, C., 2012. Decoding multiple tectonothermal events in zircons from single rock samples: SHRIMP zircon U–Pb data from the late Neoarchean rocks of Daqingshan, North China Craton. Gondwana Res. 22, 810–827.
Makrygina, V.A., Koneva, A.A., Piskunova, L.F., 1989. Granulites of the Nyurundukan Group in northern Baikal region. Doklady Akademi Nauk 307, 195–201 (in Russian).
Makrygina, V.A., Konnikov, E.G., Neymark, L.A., Pakhol'chenko, Yu.A., Posokhov, V.F., Sandimirova, G.P., Tomilenko, A.A., Tsygankov, A.A., Vrublevskaya, T.T., 1993. The age of granulite-charnockite complex of Nurundyukan Suite, northern Cisbaikalia (paradox of radiochronology). Doklady Academi Nauk 332, 486–490 (in Russian).
Möller, A., O'Brien, P.J., Kennedy, A., Kröner, A., 2003. Linking growth episodes of zircon and metamorphic textures to zircon chemistry: an example from the ultrahigh-temperature granulites of Rogaland (SW Norway). Geol. Soc. Lond., Special Publ. 220, 65–81.
Moser, D.E., Cupelli, C.L., Barker, I.R., Flowers, R.M., Bowman, J.R., Wooden, J., Hart, J.R., 2011. New zircon shock phenomena and their use for dating and reconstruction of large impact structures revealed by electron nanobeam (EBSD, CL, EDS) and isotopic U–Pb and (U–Th)/He analysis of the Vredefort dome. Can. J. Earth Sci. 48, 117–139.
Moser, D.E., Davis, W.J., Reddy, S.M., Flemming, R.L., Hart, R.J., 2009. Zircon U–Pb strain chronometry reveals deep impact triggered flow. Earth Planet. Sci. Lett. 277, 73–79.
Nasdala, L., Hofmeister, W., Norberg, N., Mattinson, J.M., Corfu, F., Dörr, W., Kamo, S.L., Kennedy, A.K., Kronz, A., Reiners, P.W., Frei, D., Kosler, J., Wan, Y., Götze, J., Häger, T., Kröner, A., Valley, J.W., 2008. Zircon M257 – a homogeneous natural reference material for the ion microprobe U–Pb analysis of zircon. Geostand. Geoanal. Res. 32, 247–265.
Neymark, L.A., Rytsk, E.Yu., Rizvanova, N.G., Gorokhovsky, B.M., 1993. Multistage formation of the Angara-Vitim Batholith: evidence from U–Pb zircon and titanite data. Doklady Akademi Nauk 333, 634–637 (in Russian).
Nekrasov, G.E., Makeev, A.F., 2003. The U–Pb Zircon Age of plagiogranite from the plagiogranite–amphibolite complex of the Ganychalan Block, western Koryak Highland. Trans. (Doklady) Russ. Acad. Sci. Earth Sci. Sect. 390, 574–576.
Nekrasov, G.E., Rodionov, N.V., Berezhnaya, N.G., Sergeev, S.A., Ruzhentsev, S.V., Minina, O.R., Golionko, B.G., 2007. U–Pb Age of zircons from plagiogranite veins in migmatized amphibolites of the Shaman Range (Ikat-Bagdarin zone, Vitim Highland, Transbaikal region). Dokl. Earth Sci. 413, 160–163.
Nekrasov, G.E., Bogomolov, E.S., 2015. Ophiolites of the Ust-Belskii terrane (Chukotka): A consequence of late Lrecambrian breakup of the Rodinia supercontinent in structures of the NE framing of the Siberian craton (structural, petrological-mineralogical, and isotope data). Dokl. Earth Sci. 461, 351–355.
Nelson, D.R., 1997. Compilation of SHRIMP U–Pb Zircon Geochronology Data, 1996. Geological Survey of Western Australia, Record 1997/2, 189pp.
Nemerov, V.K., Stanevich, A.M., 2001. Evolution of the Riphean–Vendian biolithogenic settings in the Baikal mountainous area. Geol. Geofiz. 42, 456–470 (in Russian).
Orlova, A.V., Anosova, M.O., Fedotova, A.A., Kostitsyn, Yu.A., 2012. Crystallization age of zircon from enderbite–granulite association of northern Baikal region. In: Laverov, N.P., Chernyshev, I.V. (Eds.), Proceedings of 5th Russian Conference on Isotopic Geochronology: Geochronometric Isotopic Systems, Research Methods, and Chronology of Geological Processes. Institute of Geology of Ore Deposits (IGEM), Russian Academy of Sciences, Moscow, pp. 265–268.
Parfenov, L.M., Badarch, G., Berzin, N.A., Hwang, Duk Hwan, Khanchuk, A.I., Kuzmin, M.I., Nokleberg, W.J., Obolenskiy, A.A., Ogasawara, M., Prokopiev, A.V., Rodionov, S.M., Smelov, A.P., Yan, Hongquan, 2010. In: Nokleberg W.J. (Ed.), Metallogenesis and Tectonics of Northeast Asia. United States Geological Survey, Professional Paper 1765, 1–36pp.
Perelyaev, V.I., 2003. Ultramafic-Mafic Complexes of the Western Part of the Middle-Vitim Mountain System. Unpublished Candidate of Science Dissertation. Institute of the Earth's Crust, Siberian Branch, Russian Academy of Sciences, Irkutsk, 159pp (in Russian).
Pfänder, J.A., Jochum, K.P., Kozakov, I., Kröner, A., Todt, W., 2002. Coupled evolution of back-arc and island arclike mafic crust in the late Neoproterozoic Agardagh Tes-Chem ophiolite, Central Asia: evidence from trace element and Sr–Nd–Pb isotope data. Contrib. Miner. Petrol. 143, 154–174.
Rimša, A., Whitehouse, M.J., Johansson, L., Piazolo, S., 2007. Brittle fracturing and fracture healing of zircon: an integrated cathodoluminescence, EBSD, U–Th–Pb and REE study. Am. Mineral. 92, 1213–1224.
Ruzhentsev, S.V., Minina, O.R., Aristov, V.A., Golionko, B.G., Larionov, A.N., Lykhin, D.A., Nekrasov, G.E., 2010. Geodynamics of the Eravna zone (Uda-Vitim fold system of the Transbaikal region): geological and geochronological data. Dokl. Earth Sci. 434, 1168–1171.
Ruzhentsev, S.V., Minina, O.R., Nekrasov, G.E., Aristov, V.A., Golionko, B.G., Doronina, N.A., Lykhin, D.A., 2012. The Baikal-Vitim fold system: structure and geodynamic evolution. Geotectonics 46, 87–110.
Rytsk, E.Yu., Amelin, Yu V., Rizvanova, N.G., et al., 2001a. Age of rocks in the Baikal–Muiya foldbelt. Stratigr. Geol. Correl. 9, 315–326.
Rytsk, E.Yu., Kovach, V.P., Makeev, A.F., Bogomolov, E.S., Rizvanova, N.G., 2009. The eastern boundary of the Baikal collisional belt: geological, geochronological, and Nd isotopic evidence. Geotectonics 43, 264–273.
Rytsk, E.Yu., Amelin, Yu.V., Rizvanova, N.G., Krymskii, R.Sh., Mitrofanov, G.L., Mitrofanova, N.N., Perelyaev, V.I., Shalaev, V.S., 2001b. Age of rocks in the Baikal–Muya foldbelt. Stratigr. Geol. Correl. 9, 315–326.
Rytsk, E.Yu., Kotov, A.B., Andreev, A.A., Yarmolyuk, V.V., Velikoslavinskii, S.D., Kovach, V.P., Makeev, A.F., Fedoseenko, A.M., 2013. The structure and age of the Baikal granitoid massif: new evidence for early Baikalian events in the Baikal–Muya mobile belt. Dokl. Earth Sci. 453, 1205–1208.
Rytsk, E.Yu., Kovach, V.P., Kovalenko, V.I., Yarmolyuk, V.V., 2007. Structure and evolution of the continental crust in the Baikal fold region. Geotectonics 41, 440–464.
Rytsk, E.Yu., Kovach, V.P., Yarmolyuk, V.V., Kovalenko, V.I., Bogomolov, E.S., Kotov, A.B., 2011. Isotopic structure and evolution of the continental crust in the East Transbaikalian segment of the Central Asian Foldbelt. Geotectonics 45, 349–377.
Salop, L.I., 1964. Geology of the Baikal Mountain Region. Nedra Publishing House, Moscow, 515p (in Russian).
Schaltegger, U., Fanning, C.M., Gunther, D., Maurin, D.C., Schulmann, K., Gebauer, D., 1999. Growth, annealing and recrystallization of zircon and preservation of monazite in high-grade metamorphism: conventional and in situ U–Pb isotope, cathodoluminescence and microchemical evidence. Contrib. Miner. Petrol. 134, 186–201.
Shatskii, V.S., Jagoutz, E., Ryboshlyakov, Y.V., Kozmenko, O.A., Vavilov, M.A., 1996. Eclogites of the North-Muya block – evidence for Vendian collision in the Baikal–Muya ophiolite belt. Doklady Akademi Nauk 350, 677–680 (in Russian).
Shatsky, V.S., Sitnikova, E.S., Tomilenko, A.A., Ragozin, A.L., Koz'menko, O.A., Jagoutz, E., 2012. Eclogite–gneiss complex of the Muya block (East Siberia): age, mineralogy, geochemistry, and petrology. Russ. Geol. Geophys. 53, 501–521.
Shervais, J.W., 1983. Ti–V plots and the petrogenesis of modern and ophiolitic lavas. Earth Planet. Sci. Lett. 59, 101–118.
Sovetov, J.K., Kulikova, A.E., Medvedev, M.N., 2007. Sedimentary basins in the southwestern Siberian Craton: late Neoproterozoic-Early Cambrian rifting and collisional events. Geol. Soc. Am., Special Papers 423, 549–578.
Sovetov, J.K., 2011. Neoproterozoic Sedimentary Basins: Stratigraphy, Geodynamics and Petroleum Potential. Guidebook on the Post-Conference Field trip to the East Sayan Foothills. Novosibirsk: Institute of Geology and Geophysics, Siberian Branch, Russian Academy of Sciences, 229pp.
Stanevich, A.M., Perelyaev, V.I., 1997. On late Precambrian stratigraphy of the Middle-Vitim mountain system (Delyun-Uranskii Range). Russ. Geol. Geophys. 38, 1642–1652.
Stanevich, A.M., Mazukabzov, A.M., Postnikov, A.A., Nemerov, V.K., Pisarevsky, S.A., Gladkochub, D.P., Donskaya, T.V., Kornilova, T.A., 2007. Northern segment of the Paleoasian Ocean: neoproterozoic deposition history and geodynamics. Russ. Geol. Geophys. 48, 46–60.
Taylor, S.R., McLennan, S.M., 1985. The Continental Crust: its Composition and Evolution. Blackwell Scientific Publications, London, 312pp.
Terenteva, L., Kovach, V.P., Yarmolyuk, V.V., Kovalenko, V.I., Kozlovsky, A.M., 2008. Composition, sources, and geodynamics of rock formation in the Late Riphean Bayankhongor ophiolite zone: characteristics of early stages in the evolution of the Paleo-Asian Ocean. Dokl. Earth Sci. 423A, 1462–1466.
Tikhomirov, P.L., 2010. Age of plagiogranite from the Ust-Belaya ophiolite complex (western Koryak folded zone): evidence from SHRIMP U–Pb dating of zircons. Dokl. Earth Sci. 434, 1362–1365.
Tsygankov, A.A., 2005. Magmatic Evolution of the Baikal–Muya Volcano-Plutonic belt in the late Precambrian. Publishing House, Siberian Branch. Russian Academy of Sciences, Novosibirsk, 306pp. (in Russian).
Tsygankov, A.A. 1996. Mineralogy and thermometry of the granulite-charnockite complex in the northern Baikal region. Proceedings of the Russian Mineralogical Society (Zapiski VMO) 125, 38–48 (in Russian, with English abstract).

Turkina, O.M., Nozhkin, A.D., Bibikova, E.V., Zhuravlev, D.Z., Travin, A.V., 2004. The Arzybei Terrane: a fragment of the Mesoproterozoic island-arc crust in the southwestern framing of the Siberian craton. Dokl. Earth Sci. 395, 246–250.

Vavra, G., Gebauer, D., Schmid, R., Compston, W., 1996. Multiple zircon growth and recrystallization during polyphase Late Carboniferous to Triassic metamorphism in granulites of the Ivrea zone (southern Alps): an ion microprobe (SHRIMP) study. Contrib. Miner. Petrol. 122, 337–358.

Vernikovsky, V.A., 1996. Geodynamic Evolution of the Taimyr Folded Area. United Institute of Geology, Geophysics and Mineralogy, Siberian Branch, Russian Academy of Sciences, Novosibirsk, 202pp. (in Russian with English Abstract).

Vernikovsky, V.A., Vernikovskaya, A.E., 2001. Central Taimyr accretionary belt (Arctic Asia): meso-neoproterozoic tectonic evolution and Rodinia breakup. Precambr. Res. 110, 127–141.

Wan, Y.S., Liu, D.Y., Dong, C.Y., Liu, S.J., Wang, S.J., Yang, E.X., 2011. U–Th–Pb behavior of zircons under high-grade metamorphic conditions: a case study of zircon dating of meta-diorite near Qixia, eastern Shandong. Geosci. Front. 2, 137–146.

Wiedenbeck, M., Allé, P., Corfu, F., Griffin, W.L., Meier, M., Oberli, F., von Quadt, A., Roddick, J.C., Spiegel, W., 1995. Three natural zircon standards for U–Th–Pb, Lu–Hf, trace element and REE analyses. Geostandard Newslett. 19, 1–23.

Wilhem, C., Windley, B.F., Stampfli, G.M., 2012. The Altaids of Central Asia: a tectonic and evolutionary innovative review. Earth-Sci. Rev. 113, 303–341.

Williams, I.S., 1998. U–Th–Pb geochronology by ion microprobe. In: McKibben, M.A., Shanks, III, W.C., Ridley, W.I. (Eds.), Applications of Microanalytical Techniques to Understanding Mineralizing Processes. Reviews in Economic Geology, 7, pp. 1–35.

Yarmolyuk, V.V., Budnikov, S.V., Kovalenko, V.I., Antipin, V.S., Goreglyad, A.V., Sal'nikova, E.B., Kotov, A.B., Kozakov, I.K., Kovach, V.P., Yakovleva, S.Z., Berezhnaya, N.G., 1997. Geochronology and geodynamic setting of the Angara-Vitim batholith. Petrology, 401–414.

Zorin, Yu.A., Belichenko, V.G., Turutanov, E.Kh., Mazukabzov, A.M., Sklyarov, E.V., Mordvinova, V.V., 1995. Int. Geol. Rev. 37, 154–175.